Novel Thermally-Stable $Sr_4Zn_2W_2O_{12}$: Sm^{3+} Phosphors Synthesis, Optical Properties and Applications in WLEDs

A THESIS
SUBMITTED IN PARTIAL FULFILMENT OF THE REQUIREMENTS FOR THE AWARD OF THE DEGREE OF

MASTER OF SCIENCE

IN

PHYSICS

SUBMITTED BY:

TANYA DANG (24/MSCPHY/06)

JAYA CHANDRA (24/MSCPHY/32)

Under the supervision of

Prof. Shailesh Narain Sharma

DEPATMENT OF APPLIED PHYSICS

DELHI TECHNOLOGICAL UNIVERSITY

(Formerly Delhi College of Engineering) Bawana Road Delhi- 110042

CANDIDATES'S DECLARATION

We hereby certify that the Project Dissertation titled " **Novel Thermally-Stable $Sr_4Zn_2W_2O_{12}$: Sm^{3+} Phosphors: Synthesis, Optical Properties and Applications in WLEDs** " which is submitted by, TANYA DANG (2K24/MSCPHY/06) and JAYA CHANDRA (2K24/MSCPHY/32), Department of Applied Physics, Delhi Technological University, Delhi in partial fulfillment of the requirement for the award of the degree of Master of Science, is a record of the project work carried out by the students under our supervision.

To the best of our knowledge, this work has not been submitted in part or full for any Degree or Diploma to this University or elsewhere.

Place: Delhi

TANYA (2K24/MSCPHY/06)

Date: 29 MAY 2026

JAYA (2K24/MSCPHY/32)

DELHI TECHNOLOGICAL UNIVERSITY

(Formerly Delhi College of Engineering)
Shahbad Daulatpur, Main Bawana Road, Delhi 110042

CERTIFICATE

Cerified that the TANYA DANG (24/MSCPHY/06) and JAYA CHANDRA (24/MSCPHY/32) have carried out their search work presented in this thesis entitled "**Novel Thermally-Stable $Sr_4Zn_2W_2O_{12}$: Sm^{3+} Phosphors: Synthesis, Optical Properties and Applications in WLEDs**" for the award of the degree of Master of Science from Department of Applied Physics, Delhi Technological University, Delhi under my supervision. The thesis embodies results of original work, and studies are carried out by the students themselves and the contents of the thesis do not form the basis for the award of any other degree to the candidates or to anybody else from this or any other University/Institution.

DATE: 29 MAY 2026

Prof. Shailesh Narain Sharma

Department of Applied Physics
Delhi Technological University, Delhi,
India

ACKNOWLEDGEMENT

We extend our heartfelt gratitude to our supervisor, Prof. A. S. Rao and Shailesh Nrain Sharma (Department of Applied Physics), for granting us the invaluable opportunity to work in the Materials and Atmospheric Science Research Laboratory. His exceptional guidance, unwavering support, and insightful feedback have been instrumental in the completion of this work. We deeply appreciate his valuable time, thoughtful suggestions, and meticulous review of our manuscripts. His patience and dedication during the writing process have taught us essential nuances that we will carry forward. Prof. Rao's inspiring approach to scientific inquiry made this research journey both enriching and enjoyable.

We are also highly grateful to Ms. Kanika Kardam for her guidance and unwavering support in this journey. We're grateful to the lab staff for fostering conducive and healthy working environment, which played a vital role in the success of this project. Additionally, we extend our sincere thanks to Ms. Sheetal Kumari and the faculty members, M.Sc. (Physics) scholars, and members of the Department of Applied Physics, Delhi Technological University, for their encouragement, suggestions, and valuable support throughout.

Finally, we would like to express our deepest appreciation to our parents for the unwavering belief in us and their constant encouragement, which has been our greatest source of strength and motivation.

CONTENTS:

LIST OF FIGURES

LIST OF FIGURES (continued)

LISTOF TABLES:

ABSTRACT

A series of reddish-orange emitting Sm^{3+} doped phosphors based strontium zinc tungstate $Sr_4Zn_2W_2O_{12}:xSm^{3+}$(x=3, 5, 7 and 9 mol%) host were successfully synthesised via solid state reaction route. XRD analysis confirmed synthesis of highly crystalline lattice, indicating that dopant ions were successfully integrated into tungstate host lattice matching with standard JCPDS card no.96-156-3084. Scanning electron microscopy along with Fourier transform infrared spectroscopy characterizations provide insights into the micro structural irregular polyhedron morphology and used for identifying chemical bonds respectively. The optical band gap of $Sr_4Zn_2W_2O_{12}$ phosphors at optimize concentration x=7mol% was identified to be E_g=3.71 eV through diffuse reflectance spectroscopy (DRS). Optical investigation via photoluminescence (PL) studies a prominent excitation peak at 406 nm, under this excitation the phosphor exhibits a highly pure reddish-orange radiation recorded at 645 nm showing $^4G_{5/2}\rightarrow{}^6H_{9/2}$ energy transfer. At an optimal doping level, x=7 mol% concentration quenching phenomenon identified. The optimized phosphor showed CIE chromaticity coordinates (0.596, 0.401) along with outstanding colour purity of 99.99% and correlated color temperature (CCT) of 1625K thus making it suitable for reddish-orange emission This optimized material exhibited exceptional color purity of 99.99%, correlated color temperature (CCT) of 1625 K and CIE chromaticity coordinates (0.596, 0.401), making it appropriate for reddish-orange emission. Temperature-Dependent Photoluminescence (TDPL) results highlighted the materials robust thermal stability with retaining 76.43% emission intensity at 175ºC, activation energy to be ΔE= 0.399 eV and quantum efficiency to be 76.9%. The results suggesting that $Sr_4Zn_2W_2O_{12}:xSm^{3+}$ is a superior host for developing high performance w-LEDs.

CHAPTER 1: INTRODUCTION

Light serves a crucial role in advancing humanity, propelling ongoing advancements in illumination technology across various scientific and technological domains. Although Thomas Edison's incandescent lamp, invented in 1879, was a significant milestone, early lighting solutions faced major issues such as voltage distortion, short operational lifespan, high production costs, and extreme energy inefficiency. Given the modern society's requirement for lighting that is both incredibly efficient and economically feasible, researchers redirected their attention to material science. This shift resulted in the identification of phosphor materials—a century-old innovation that continues to be essential in contemporary energy-efficient technology [1].

Phosphors are the materials capable of showing luminescence upon excitation from an external source. They are capable of emitting not just any light but the light in the wavelength in the visible range of electromagnetic spectrum which is 380 to 750 nanometres. This range (300nm-750nm) of the Electromagnetic spectrum is the only part which can be sensed by the human eyes and hence are perceived in the form of various colors. Conclusively, we require some material which can execute the emission of the visible light in an efficient, cost effective, environment friendly and highly radiant.

Luminescence is a phenomenon of emission of the light from a substance not due to the presence of high temperatures but other phenomena like atomic transitions, pressure, electrical and chemical responses. The term luminescence was first introduced by Eilhard Weidemann in 1888. Derived from the Latin word lumin, meaning light, the term describes the emission of radiation by certain materials known as phosphors. This phenomenon represents a unique interaction between matter and energy. These materials, also referred to as luminophores, possess the remarkable ability to convert energy from absorbed photons into visible light. The phenomenon of luminescence can be categorized in two forms: **(i) Fluorescence and (ii)Phosphorescence.** In fluorescence, luminescence occurs almost instantaneously after the absorption of incident radiation and ceases just as quickly. Typically, the emitted radiation has a longer wavelength than the incident radiation. In contrast, phosphorescence is characterized by a delayed emission following the absorption of radiation. This delay can vary significantly, lasting from several minutes to a few hours, depending on the specific host material and activator used. [2]

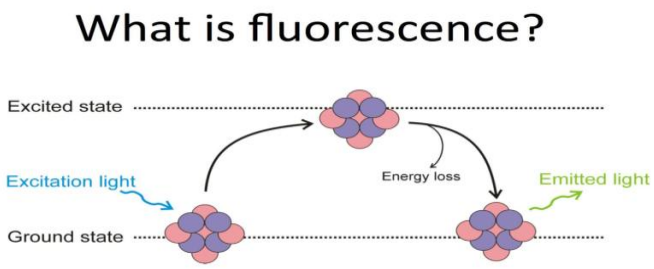

Figure 1.1: excitation and emission of light

Photoluminescence

Photoluminescence (PL) refers to the process in which a material emits light after absorbing photons (light energy). This occurrence is extensively researched in material science due to its relevance in optoelectronics, sensors, and light-emitting devices.

Figure1.2: luminescence in different colour ranges on the basis of chemical composition, phosphors can be categorized into organic and inorganic phosphors.

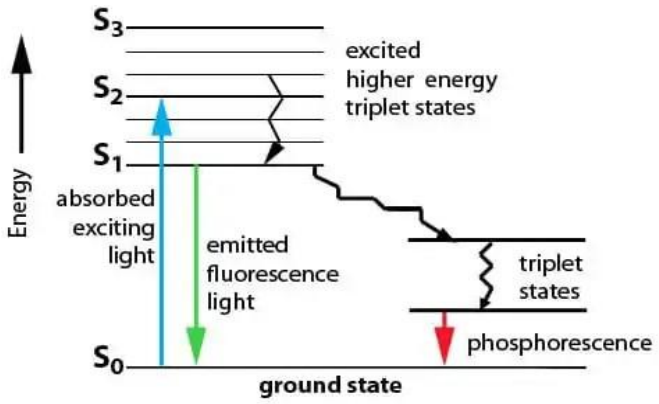

Figure 1.3: Energy level diagram for fluorescence and phosphorescence emission.

In fluorescence, a photon excites an electron within a molecule or material, promoting the electron from its ground state (S_0) to a higher energy level (S_1 or S_2). The molecule promptly dissipates vibrational energy and settles into the lowest vibrational level of the excited state (S_1). The electron subsequently returns to the ground state, releasing a photon during this transition.

Fluorescence is an extremely fast process, with emission occurring within nanoseconds (10^{-9} seconds) of photon absorption.

The emitted light generally has a longer wavelength (lower energy) than the absorbed light due to vibrational energy losses during relaxation. This is known as the **Stokes shift**.

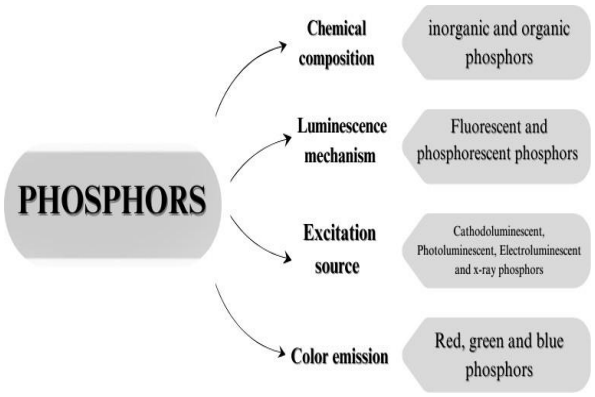

Figure 1.4: various types of phosphors.

as seen in picture 1.4. In this research, we have utilised inorganic phosphors. Phosphors can be synthesised using a variety of techniques. The integration of the activator ions into a host matrix is the fundamental idea behind the phosphor's manufacture. Synthesis is a labour-intensive procedure. A functioning laboratory with high purity maintenance in the lab rooms for synthesising high purity phosphors is necessary to conduct phosphor research. For heat treatments like calcination and sintering, the lab should have furnaces that can achieve temperatures as high as 1700C. [3,4]

Phosphor formulations often comprise more than four elements, making it challenging to produce uniform, single-phase powders. These material's luminescence efficiency is determined by their characteristics, which are impacted by elements including atomic structure.

Rare-earth element ions, sometimes referred to as transition metal ions, are the activator ions that are utilized. The illumination of phosphors at different color ranges is mainly caused by these activator ions [5].

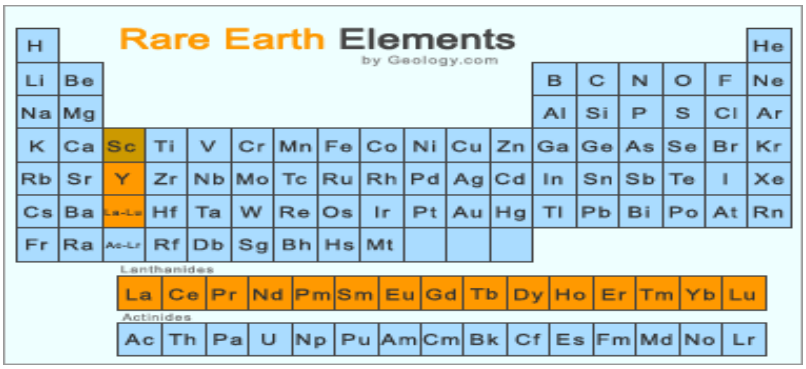

Fig1.5: Periodic table highlighted with rare earth elements.

Host matrix and activator ions for the phosphors

The Rare-earth activated phosphors have different kinds of properties. A host material is chosen

and designed in such a way that it incorporates divalent and trivalent rare-earth ions into their lattices, which are often referred to as impurities or activator ions. When exposed to UV or visible light—or another excitation source, depending on the type of phosphor—activator ions absorb the energy, transition to an excited state, and then relax to a lower energy state, emitting a photon in the process. The emitted photons usually lie in the visible wavelengths depending on the properties of the activated ions [6]. The efficiency of the phosphor is defined as the amount of energy emitted compared to the energy used to excite the material. Since some energy is lost due to Non-radiative transitions as well, hence the efficiency of phosphors is not 100%.

White LEDs (WLEDs):

The Need and Synthesis of White LEDs in Material Sciences:

White light-emitting diodes (LEDs) have revolutionized lighting technology, offering energy efficiency, durability, and eco-friendliness compared to traditional incandescent and fluorescent lighting. ‘’’The growing demand for sustainable and high-performance lighting solutions has driven extensive’ research into the development of white LEDs in material science. The need for white LEDs stems from their superior energy efficiency, consuming up to 80% less power while offering comparable or better luminosity. Their long lifespan reduces maintenance costs and waste, making them an environmentally responsible choice. Furthermore, white LEDs exhibit high luminous efficacy, rapid response times, and excellent reliability, making the mind is pens able for applications in residential, industrial, and automotive lighting, as well as in display technologies [7–9].

The synthesis of white LEDs involves two primary approaches: **phosphor-based** and **phosphor-free** methods.

In phosphor-based white LEDs: a blue or ultraviolet LED excites a phosphor material, typically rare-earth-doped compounds such as YAG:Ce (yttrium aluminum garnet doped with cerium), to produce white light. This approach is widely used due to its simplicity and efficiency, although it may face limitation sin achieving high color rendering index (CRI) and thermal stability. Researchers are actively exploring alternative phosphor compositions, such as silicates, nitrides, and oxynitrides, to overcome these challenges [7–10].

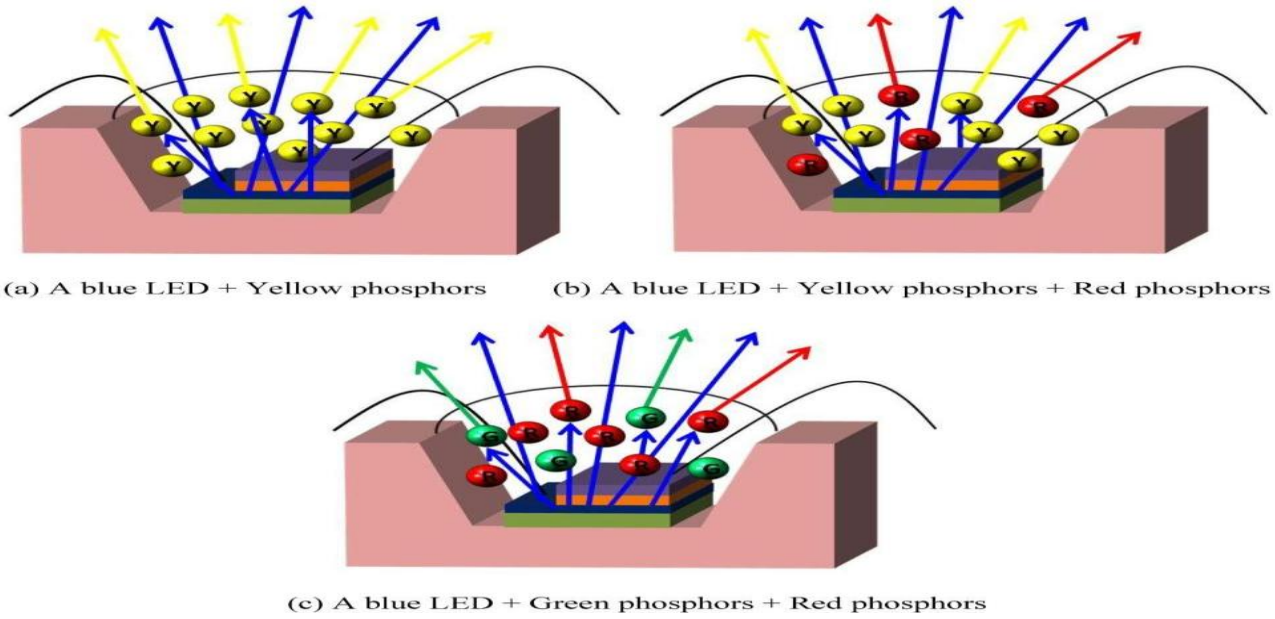

Figure1.6: the different approaches for white light production.

Phosphor-free methods, on the other hand, generate white light by combining red, green, and blue (RGB) LEDs. This approach enables precise control over the emitted spectrum, resulting in superior color rendering and tunability. However, balancing the intensity and stability of individual LEDs remains a challenge, requiring innovations in material engineering.

Some **parameters** are crucial to analyse in the white LEDs synthesized such as:

CRI (Color Rendering Index):

Applications:

High CRI (90+): Required in applications like photography, art galleries, medical lighting, and retail.

Moderate CRI (70–89): Suitable for general residential, commercial, or office lighting.

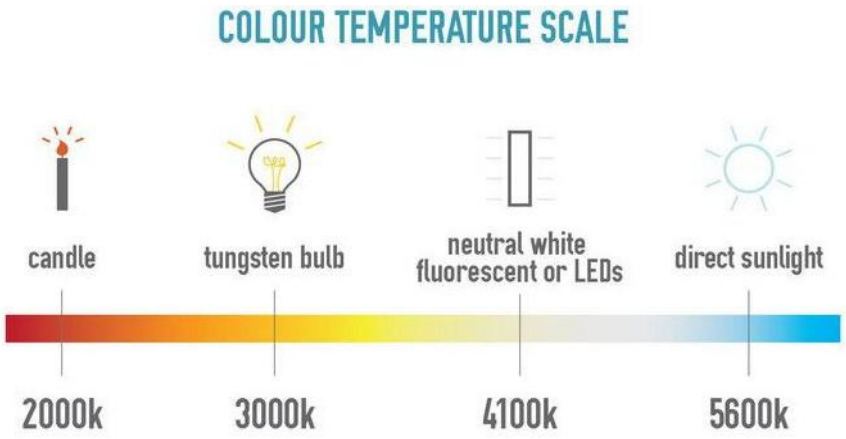

Figure1.7: the temperatures depicting the quality of white light produced by different sources. The Common CCT values range from 2700 K (warm white) to 6500 K (daylight white).

CCT (Correlated Color Temperature):

Definition: CCT describes the color appearance of the light emitted by a source, measured in Kelvin (K). It indicates whether the light appears warm (yellowish) or cool (bluish).

CCT Scale:(seefigure1.7)

Warm White (2000–3000K): Produces a cozy, inviting yellowish light. Commonly used in homes, restaurants, and hotels.

Neutral White (3100–4500K): Balanced light with a neutral tone, suitable for offices and retail spaces.

Cool White (4600–6500 K): Bright, bluish-white light that mimics daylight. Used in hospitals, industrial areas, and outdoor spaces.

Applications: Choosing the right CCT enhances the ambiance and functionality of a space. For instance, warm white is preferred for relaxation, while cool white improves focus and visibility.

Both **CRI** and **CCT** are critical parameters for assessing and optimizing the quality of light in LED-based applications.

In material science, the development of white LEDs focuses on optimizing the performance of luminescent materials and improving energy efficiency. Key research areas include enhancing thermal stability, minimizing non-radiative energy losses, and increasing quantum efficiency. Additionally, the integration of nano materials and advanced fabrication techniques offers promising pathways for achieving higher efficiency and stability in next-generation white LEDs [12–14].

Figure1.8: The common characteristics of a white LED.

White LEDs represent a remarkable confluence of scientific innovation and environmental responsibility. As material science continues to advance, white LED technology is set to play a pivotal role in creating sustainable, energy-efficient lighting solutions for a brighter and greener future.

Chapter 2: Instrumentation

X-Ray Diffraction:

X-ray diffraction (XRD) is an effective analytical method used to examine the atomic and molecular arrangement of crystalline substances. This technique relies on the principle of diffraction, which takes place when X-rays collide with a crystal lattice. The resulting scattered X-rays create a pattern that offers important insights into the material's structure, phases, and characteristics.

Principle of working XRD:

X-ray diffraction operates based on Bragg's Law, which explains the constructive interference of X-rays that are reflected from parallel planes within a crystal [13].

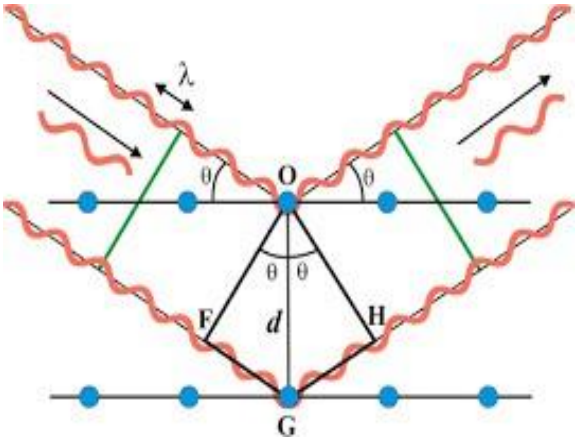

Figure2.1: The **Bragg's law** depicting the diffraction of X-rays from a crystalline plane.

Process of XRD:

1. **X-ray Generation**: X-rays are produced in an X-ray tube, where high-energy electrons bombard a metal target (commonly Cu or Mo).
2. **Sample Interaction**: The focused X-ray beam is aimed at the crystalline sample. This interaction generates scattered X-rays that depend on the lattice structure of the crystal.

3. **Detection**: A detector records the intensity of diffracted X-rays as a function of the diffraction angle (2θ).
4. **Data Analysis**: Information about the crystal structure, phase composition, and other characteristics is extracted from the diffraction pattern, which is made up of peaks that correspond to particular crystal planes. [7,13,15]

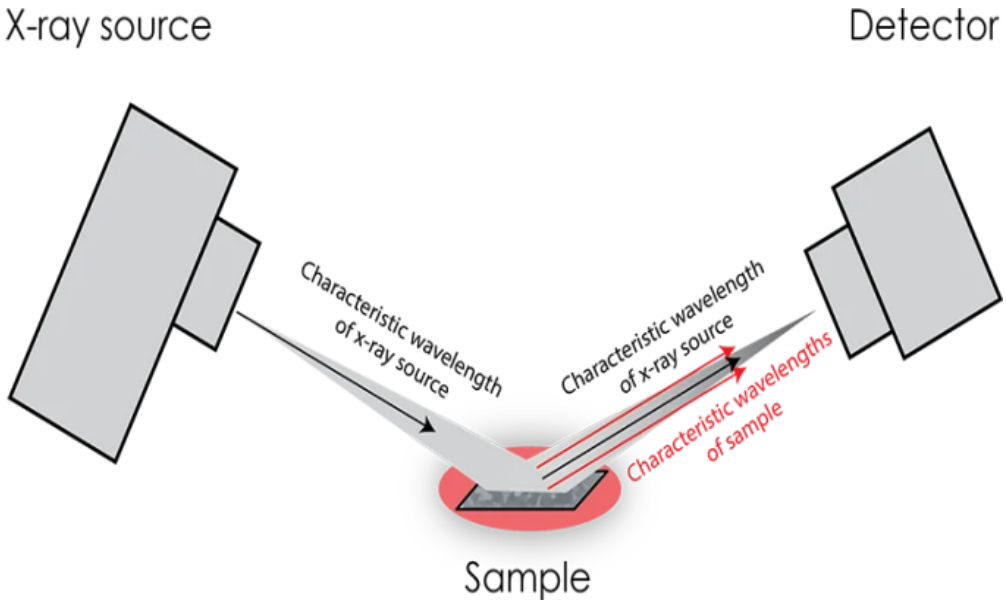

Figure2.2: The principle working of X-ray diffractometer.

XRD Applications: Material science, geology, chemistry, and engineering all make substantial use of XRD. It assists in determining lattice constants, identifying crystalline phases, analyzing crystallite size, and detecting structural flaws. XRD is an important tool for researching both natural and manmade materials, including minerals, metals, medicines, and polymers. It is precise and non-destructive.

This method has significantly improved our comprehension of the characteristics and behavior of materials.

How an X-Ray Diffractometer (XRD) Machine Operates: An X-ray diffractometer (XRD) is a potent analytical instrument used to ascertain the lattice parameters, phase composition, and crystalline structure of materials. Bragg's Law, which links the diffraction of X-rays by crystal planes to their spacing, is the foundation of its operation.

● X-Ray Generation: In an X-ray tube, X-rays are first produced. High-voltage electrons accelerated with a target material (usually copper or molybdenum), producing X-rays via unique emission mechanisms and Bremsstrahlung. The sample is the target of these collimated X-rays.

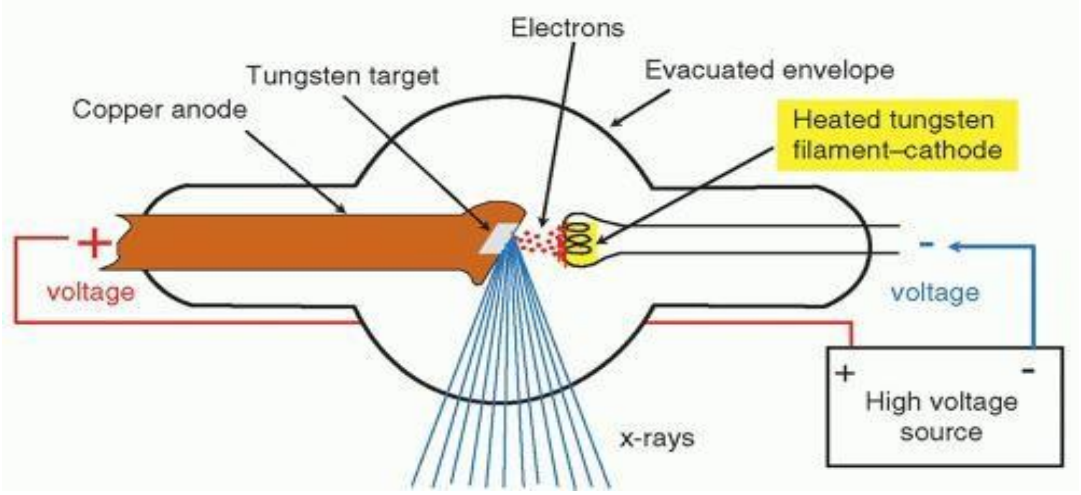

Figure2.3: The X-Ray tube

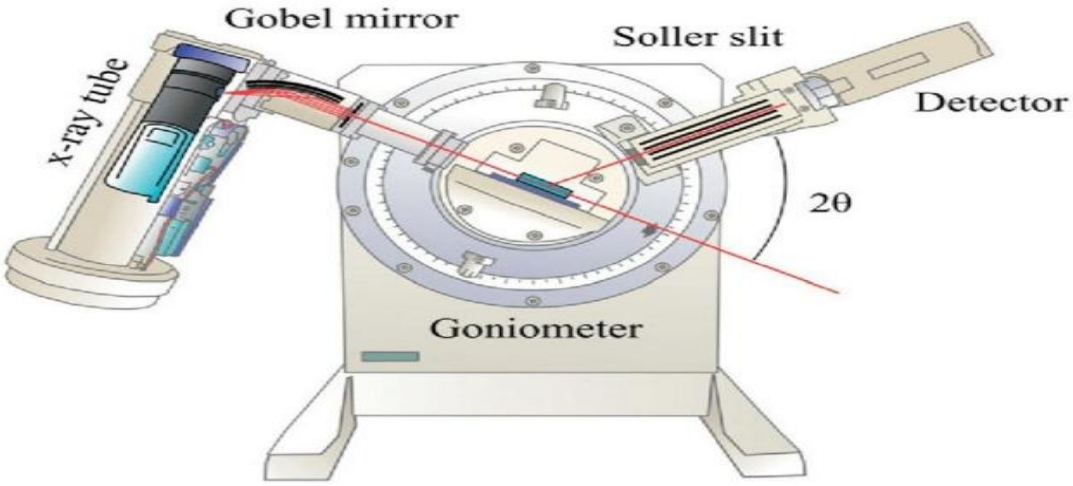

Figure2.4: The X-Ray diffractometer machine

Usually in thin-film or powder form, the sample is placed on a holder. The crystal planes function as diffraction gratings when the collimated X-ray beam hits the crystalline sample, scattering the X-rays in particular directions. The scattered X-rays cause interference.

Either constructively or destructively, depending on the incidence angle and the crystal plane separation. Bragg's Law is followed by constructive interference [16, 17].

$$n\lambda = 2d\sin\theta \qquad (1)$$

Where n is the order of diffraction, λ is the X-ray wavelength, d is the inter planar spacing, and θ is the diffraction angle.

Detector and Data collection

The intensity of diffracted X-rays at different angles (2θ) is recorded by a detector that is positioned to revolve around the sample. Plotting intensity against angle, the resulting diffraction pattern has peaks that represent distinct crystal planes.

The crystal structure, phase composition, and other characteristics of the material are determined by analyzing the diffraction pattern. To identify the material, software programs compare the patterns with relevant databases.

Data Analysis

The crystal structure, phase composition, and other characteristics of the material are determined by the diffraction pattern. To identify the substance, software programs compare the patterns with relevant databases.

In materials science, geology, chemistry, and engineering, XRD is used to characterize crystalline materials and comprehend their structural characteristics. It is a non-destructive, precise, and versatile technique.

X-ray diffraction (XRD) analysis provides a wealth of information about the structural and physical properties of crystalline materials. The key depictions that can be drawn from XRD data include:

1.PhaseIdentification

What It Shows: Different diffraction peaks that correspond to the crystal planes of particular phases are present. The crystalline phases of the material can be determined by comparing the experimental pattern with reference databases (such as ICDD).

Application: Identifying single-phase or multi-phase compositions in polymers, ceramics, minerals, and alloys.

2.Lattice Parameters

What It Shows: The unit cell dimensions (lattice constants) of the crystal may be ascertained by calculating the interplanar spacing (dd) using Bragg's Law.
Application: Verifying structural alterations like doping or alloying and comprehending crystal structures (such as cubic, tetragonal, or hexagonal).

3.Crystallite Size

What It Shows: The average size of crystallites in the material may be estimated from the width of the diffraction peaks using the Scherrer equation, which is given below.

Crystallite Size=Kλ/βcosθ

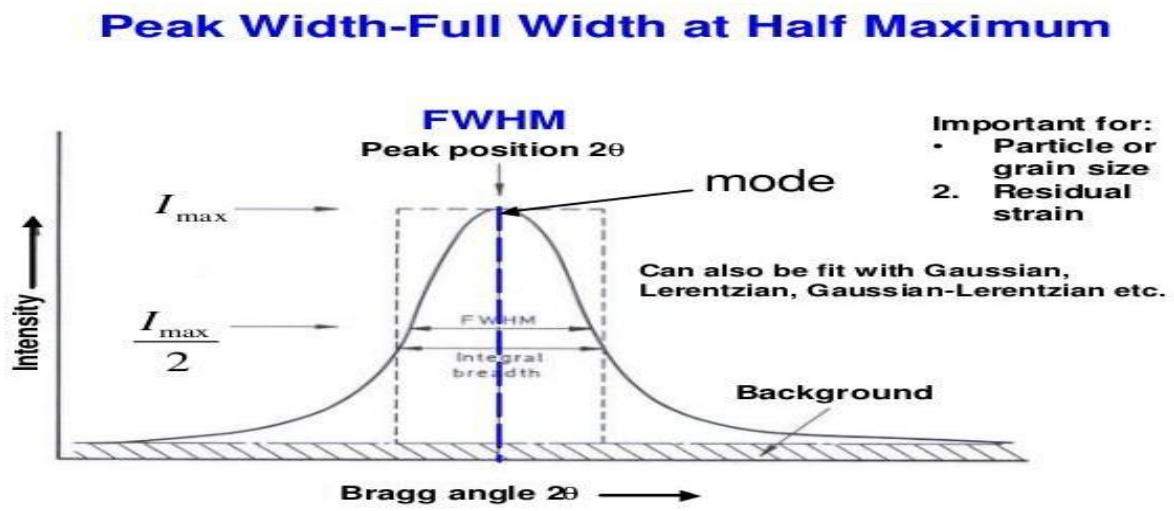

Figure2.5: Analysing a peak in XRD data plot

Where K is the shape factor, λ is the X-ray wavelength, β is the full width at half maximum (FWHM), and θ is the diffraction angle.

Application: Analysis of nanomaterials, thinfilms, and grain refinement in metals.

5.Strain and Defects:

What It Shows: The material's strain, lattice distortion, or crystal flaws are indicated by the shift, width, or asymmetry of diffraction peaks.

Application: Examining structural integrity, defect engineering in semiconductors, and residual stress in metals.

6.Preferred Orientation (Texture):

What It shows: The preferred alignment of crystallites, or texture, is reflected by anisotropy in peak intensities.

Application: Comprehending the orientation of grains in polycrystalline materials, such coatings or rolled metals.

7. Amorphous Content Identification

What It shows: The diffraction pattern reveals the presence of both crystalline and amorphous phases.

Application: Researching materials that are partly crystalline, glass, or polymers.

8. Space Groups and Symmetry

What It Shows: The symmetry and space group of the crystal structure may be ascertained by analyzing peak locations and intensities.

Application: Categorizing crystal formations and comprehending their physical characteristics.

Photoluminescence (PL) Spectroscopy:

photoluminescence (PL) spectroscopy is an optical method for examining the electrical and optical characteristics of materials. Photons, creating a non-destructive technique for characterizing photonic devices, semiconductors, and nanomaterials. Electrons in the materials are stimulated from their ground state to higher electronic energy levels when it absorbs light, usually in the ultraviolet, visible, or near-infrared spectrum. These stimulated electrons release photons as they return to their ground state following a short relaxing period. To learn more about the material's characteristics, the light that is released is examined.

Key steps in the process:

1. Excitation: Electrons in the material are excited by a light source, such as a laser or lamp.

2. Relaxation: Electrons lose energy by non-radiative or radiative (light-emitting) processes.

3. Emission: Photons released by radiative transitions are measured and examined.

Figure2.6: Photoluminescence (PL) spectrometer

Information Obtained from PL Spectroscopy:

1. Electronic Structure: In semiconductors, PL spectra provide bandgap energy, defect states, and excitonic transitions.
2. Material Quality: Broad or displaced peaks imply flaws or impurities, whereas sharp and well-defined peaks show excellent crystal quality.
3. Defect Analysis: It is possible to identify non-radiative processes and emissions from defect states.
4. Quantum Efficiency: The efficiency of photon absorption and emission is assessed using the intensity of light emitted.
5. Charge Carrier Dynamics: The time-resolved PL (TRPL) method provides light on recombination processes and carrier lifetimes.

In materials science, PL spectroscopy is a flexible and essential technique for developing next-generation photonic and optoelectronic technologies. See Figure 2.6 a UV-PL spectrometer.

The method of scanning electron microscopy (SEM):

A imaging method for examining the surface appearance and microstructure of materials at extremely high magnifications is scanning electron microscopy, or SEM. These electrons interact with the sample's atoms to produce a variety of signals, including secondary electrons, backscattered electrons, and X-rays, which are gathered to provide elemental information and detailed pictures.

Secondary electrons, which produce high-resolution, three-dimensional-like representations of the surface topography, are the most frequently discovered signals. On the other hand, backscattered electrons help in phase differentiation based on atomic number contrast. Often connected to SEM equipment, energy-dispersive X-ray spectroscopy (EDS) enables further study of particular regions.

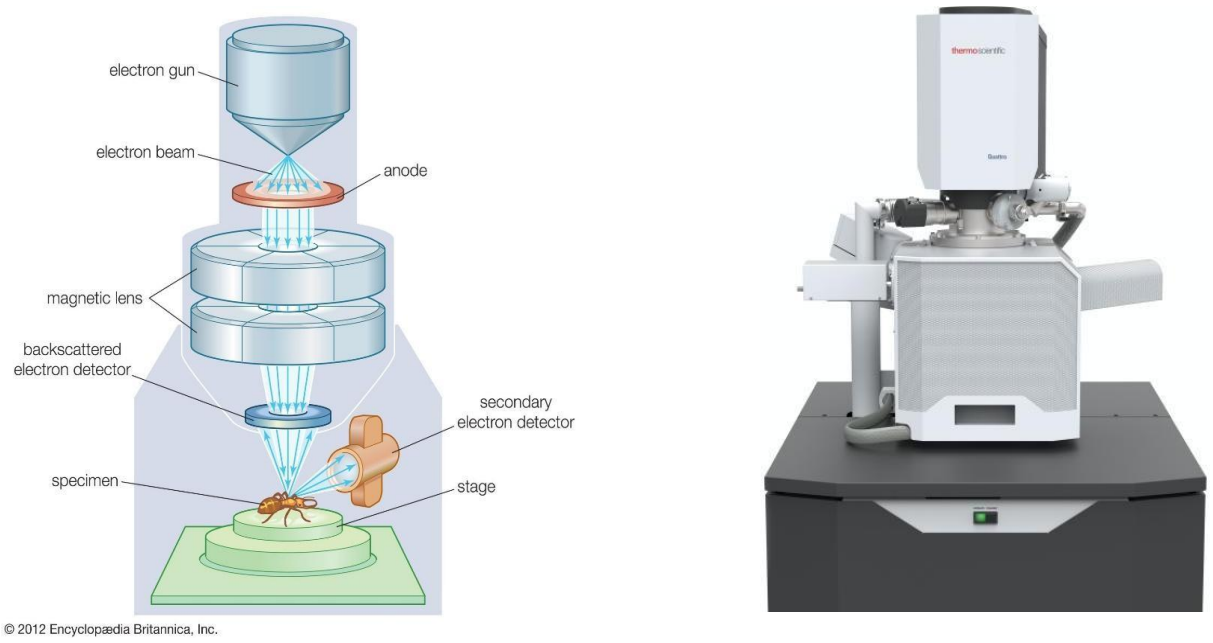

Figure 2.7: Schematic diagram of scanning electron microscopy and SEM machine

The Operation of Scanning Electron Microscopy (SEM):

1. Generation of electron beam: The first step in SEM is to create a concentrated beam of high-energy electrons using an electron cannon, which is usually composed of tungsten or a field emission source. Electromagnetic lenses are used to accelerate and narrow these electrons into a fine beam.
2. Scanning the Sample: The surface of sample is scanned in a grid-like pattern using a concentrated electron beam. To stop air molecules from scattering electrons, this interaction takes place in a vacuum chamber.
3. Electron-Sample Interaction: A types of signals are produced when the beam interacts with the atoms on the surface.
4. Secondary electrons (SE): These electrons are ejected from outer shells of the atom and provide surface topography.
5. Backscattered electrons (BSE): Provide compositional contrast by reflecting from the nucleus, making heavier elements seem brighter.
6. Characteristic X-rays: Used for elemental analysis (EDS/EDX), released when inner-shell electrons are replenished.
7. Detection and Imaging: These signals are captured by detectors, which transform them into electrical signals that are then processed to create a picture on a computer screen.

The sample must be electrically conductive for SEM. Usually, a thin layer of carbon, platinum, or gold is coated on non-conductive materials. SEM is crucial in fields like materials science, nanotechnology, biology, and semiconductor research because of its resolution, which can drop to a few nanometers [18-22]

Chapter 3 Process of synthesis

Fig.1 shows $Sr_4Zn_2W_2O_{12}$ phosphor host lattice synthesized via conventional high–temperature solid-state reaction method. High purity starting materials, specifically $SrCO_3$(99.0%), ZnO (99%), and WO_3 (99.99%) were employed as phosphors. Calculated quantities of these reagents were combined together and uniformly blended using agate mortar and pestle. Acetone added as grinding medium for homogeneous mixing and fine particle production. The obtained homogenous mixture was moved into alumina crucible and calcined in muffle furnace at temperatures 1200°C for 7 hours. Following the thermal treatment, the samples were cooled naturally to room temperature. The synthesized powders were regrind for the consistency of particle size. From this approach, Sm^{3+}-activated$Sr_4Zn_2W_2O_{12}$ phosphors were effectively produced with different dopant concentrations (x= 3,5,7 and 9 mol%).

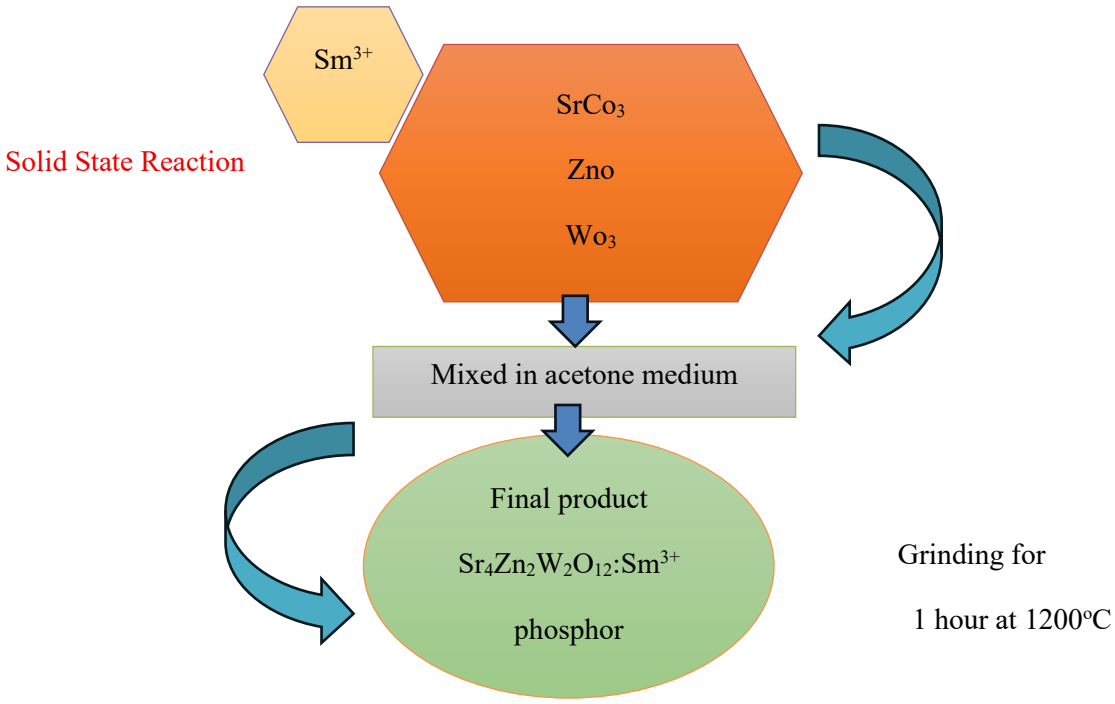

Fig.1. Flow chart of the steps involved in synthesizing of $Sr_4Zn_2W_2O_{12}$ phosphor by solid-state reaction method.

2.2. Characterization Techniques

The crystal lattice and phase homogeneity of synthesized phosphor samples were examined using XRD. A Bruker D8 advanced diffractometer based on Cu-K_α radiation (1.54 Å) filtered via

Nickel applied to record the diffraction pattern. For precise phase identification, a broad range of 2(θ) data was collected. A JOEL 7610 FSEM utilized for examine sample morphology along with specific microstructural characteristics. EDS was used simultaneously to verify the final product stoichiometric ratios and elemental composition. Using a PerkinElmer Frontier FT-IR spectrometer, Mid-infrared FT-IR spectra were recorded to identify specific functional groups and examine type of bonding within host lattice. Diffuse reflectance spectra (DRS) from the JASCO V-923 model UV-Vis-NIR spectrophotometer were employed to examine photon absorption properties regarding Sm^{3+}-doped phosphor. The JASCO FP-8300 spectrofluorometer with a xenon lamp as primary excitation source was used to measure photoluminescence (PL) parameters, including excitation and emission spectra. The luminescence durations were further verified by recording time-resolved photoluminescence decay (TRPL) profiles using an Edinburgh FL920 fluorescence spectrometer. Lastly, the Ocean Optics Flame-S-XRL-ES spectrometer was used to detect temperature-dependent PL in order to evaluate the phosphors thermal stability.

Chapter 4 Results and discussion

4.1. XRD analysis:

The XRD method was performed to evaluate the atomic arrangement structure and phase purity of both undoped and Sm^{3+}-doped$Sr_4Zn_2W_2O_{12}$phosphors.Fig. 2(a) along with 2(b) illustrate XRD patterns of $Sr_4Zn_2W_2O_{12}$:xSm^{3+} samples at different temperatures and concentration (x=0 and 7mol%) alongside the standard reference from JCPDS database card no.96-156-3084 including lattice constants a= 5.6320Å, b = 5.6080 Å, c= 9.7210Å, α =γ= 90°, β =125.36°.The XRD pattern of the undoped $Sr_4Zn_2W_2O_{12}$ phosphor at various temperatures is illustrated in Fig.1(a).The Bragg diffraction peaks are very sharp and well-defined, indicating high crystallinity, which is essential factor for luminescent efficiency. It was observed thatSm^{3+}doping does not significantly modified the host lattice framework, suggesting dopant ions are successfully incorporated into $Sr_4Zn_2W_2O_{12}$. The substitution is highly favourable due to comparable ionic radii of constituent ions; specifically, Sm^{3+} (0.958Å) can substitute for Zn^{2+} (0.74Å). The alignment of the observed diffraction peaks with the pure phase confirms that a 7 mol% doping concentration does not lead to any noticeable impurity or secondary phase represented in Fig.1(b). Using obtained XRD pattern, fundamental structural parameters, including phase identification, interplanar spacing(d) and lattice constants were determined. Furthermore, average crystallite size (D) was calculated using Debey-Scherrer equation: [23].

$$D = \frac{K\lambda}{\beta cos\theta} \qquad (1)$$

Where λ denotes X-Ray wavelength that is 1.54Å, β is FWHM, K is Scherrer constant typically taken (0.9), D represents average grain size and θ is diffraction angle.

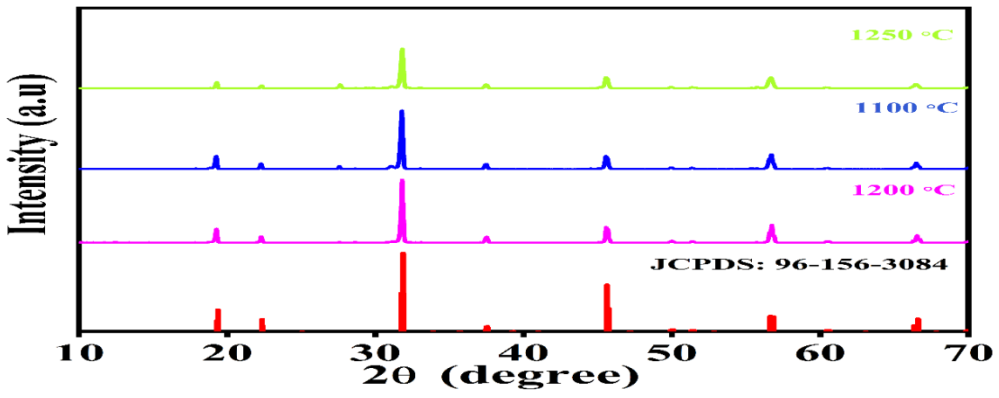

Fig. 2(a). XRD pattern at different temperatures of undoped $Sr_4Zn_2W_2O_{12}$phosphor.

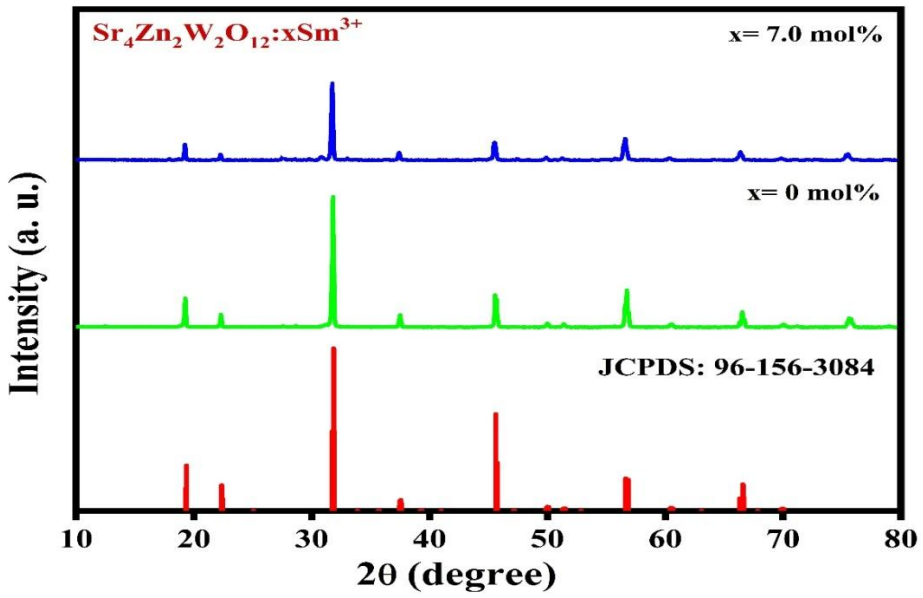

Fig.2(b). XRD pattern of $Sr_4Zn_2W_2O_{12}$:xSm^{3+} (x= 0, 7 mol%) phosphor with standard JCPDS diffraction pattern.

The calculated crystallite size of $Sr_4Zn_2W_2O_{12}$:xSm^{3+} (x=0,7 mol%) are 35.39 nm and 32.47 nm respectively. Beyond Debey-Scherrer estimation, lattice strain (ε) and crystallite size (D) of $Sr_4Zn_2W_2O_{12}$:xSm^{3+}phosphors were further evaluated using Williamson-Hall (W-H) approach. W-H relationship expressed as follows [24]:

$$\beta cos\theta = \frac{k\lambda}{D} + 4\varepsilon sin\theta \qquad (2)$$

In this approach, a linear plot is constructed with $\beta cos\theta$ on y-axis and $4sin\theta$ on x-axis. The intercept ofresulting linear fit corresponds to $\frac{k\lambda}{D}$, enabling a more refined calculation of the average crystallite size (D), while slope ofline provides value oflattice strain (ε) as shown in Fig. 2(c) [25]. Fig.2(d) represents W-H plot of $Sr_4Zn_2W_2O_{12}$:xSm^{3+}(x= 7 mol%) phosphor. The calculated crystallite size of $Sr_4Zn_2W_2O_{12}$:xSm^{3+} (x=0 and 7 mol%) by W-H approach are 80.87 nm and 90.81 nm respectively with estimated lattice strain values are 0.00125 and 0.00159. The comparatively smaller crystallite size obtained via the Debye-Scherrer equation can be attributed to its inherent limitation as it only considers size-induced peak broadening. Conversely, the Williamson-Hall method provides a more comprehensive structural assessment by decoupling the contributions of both crystallite size and microstrain to the diffraction peak width.

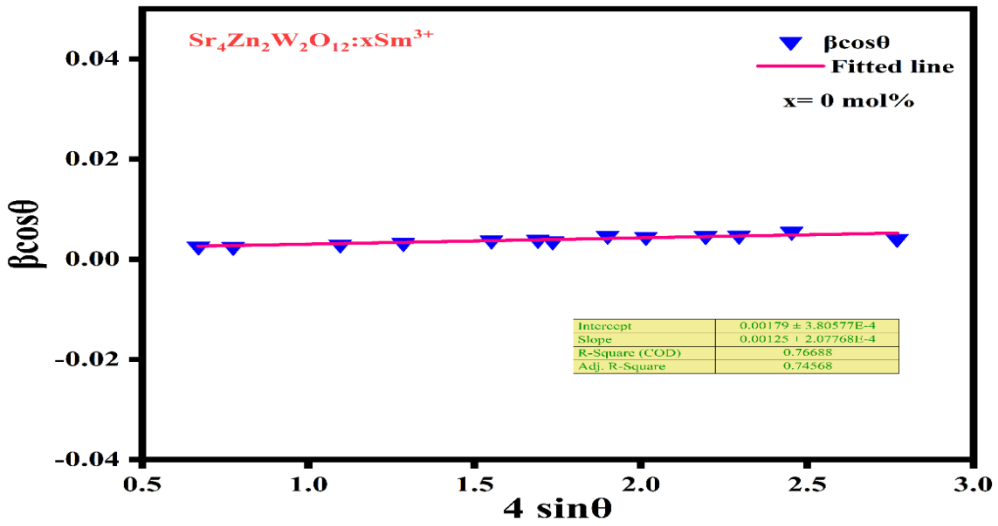

Fig.2(c). W-H plot of $Sr_4Zn_2W_2O_{12}:xSm^{3+}$(x= 0 mol%) phosphor.

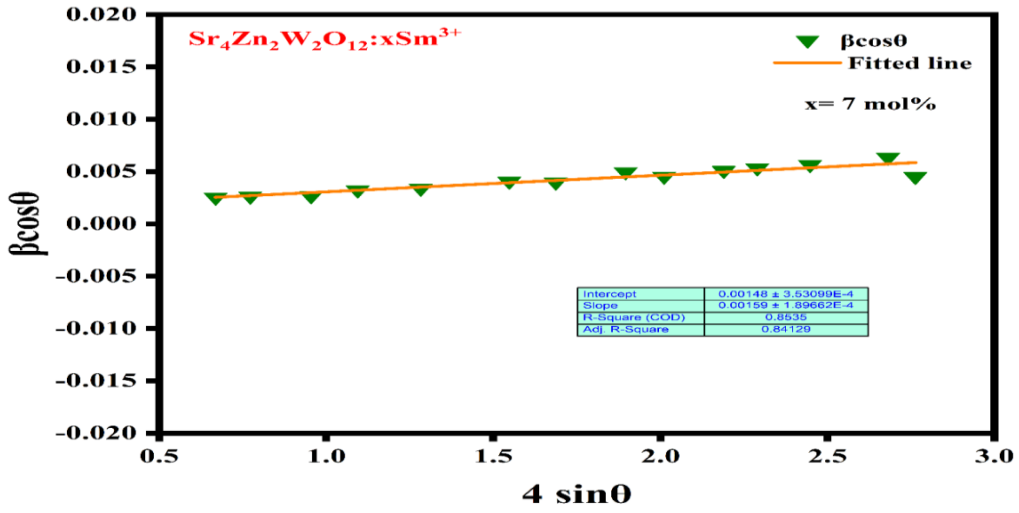

Fig.2(d). W-H plot of $Sr_4Zn_2W_2O_{12}:xSm^{3+}$(x= 7 mol%) phosphor.

The detection of microstrain in phosphor materials is generally associated with internal lattice distortions, structural imperfections, or stress arising from variations in crystallographic planes. The low strain value suggests that the $Sr_4Zn_2W_2O_{12}:Sm^{3+}$ system has relatively defect-free crystal frame and minimal lattice distortion. This implies that the stability of the host lattice structure is not affected by the addition of Sm^{3+} ions.

4.2. SEM surface analysis

SEM was utilized to investigate microstructures, morphology, topography, particle dimensions moreover size allocation of Sm^{3+}-doped phosphors. The synthesised phosphors are composed of particles with morphologies ranging from irregular polyhedron presented in Fig.3. The samples exhibit a non-uniform particle size distribution along with a moderate degree of agglomeration. This agglomeration is likely a consequence of high temperature solid state synthesis and manual grinding processes employed during preparation. The particle size for both the undoped and Sm^{3+}-activated samples was found to reside predominantly within the micrometer range such that 4µm - 10µm range respectively. These dimensions are highly comparable to commercially available phosphor materials. Such a particle size distribution is considered advantageous for the industrial coating process, as it facilitates the creation of a uniform phosphor layer, thereby enhancing the overall performance and reliability of the resulting LED devices [26].

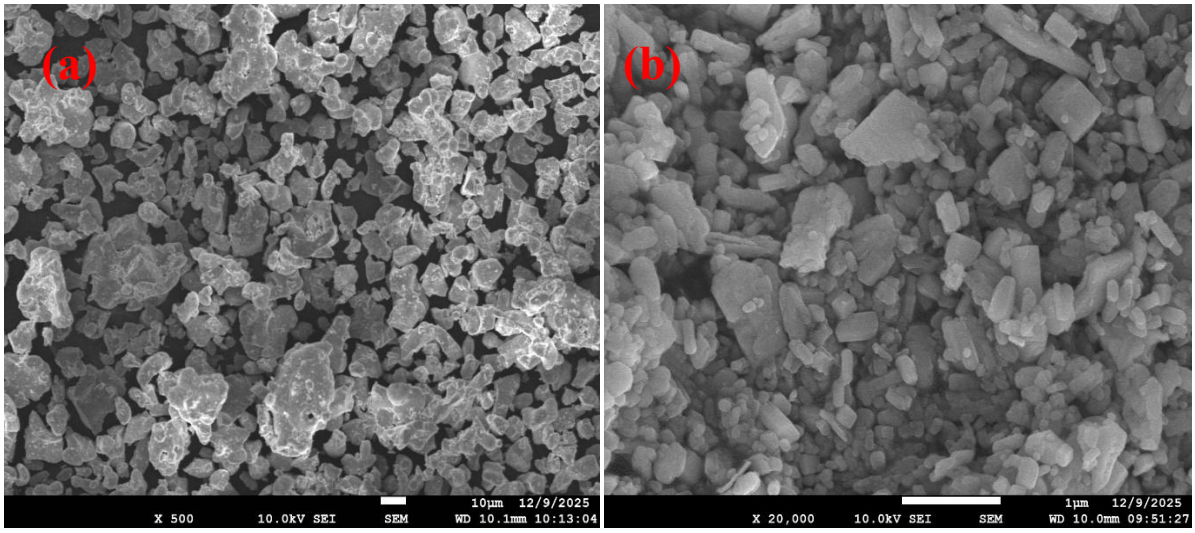

Fig.3(a) SEM images of $Sr_4Zn_2W_2O_{12}$:xSm^{3+} (x= 7 mol%) phosphor, **(b)** SEM images of undoped $Sr_4Zn_2W_2O_{12}$ phosphor.

4.3. EDS Analysis

The elemental structure and chemical composition of host lattice were verified through EDS spectroscopy. EDS spectra for a Sm^{3+}-activated sample of $Sr_4Zn_2W_2O_{12}$ phosphor at x = 7 mol% are shown in Fig.4. The analysis reveals the presence of different constituent elements such as strontium (Sr), zinc (Zn), Tungsten (W) and oxygen (O), including the samarium (Sm) dopant as the activated sample. The different peaks verify that all precursor reagents were successfully incorporated into the crystalline phosphor lattice. Additionally, the spectra validate absence of elemental impurities, confirming the high phase purity previously suggested by the XRD results.

The results provide that high-temperature solid-state reaction method successfully produced $Sr_4Zn_2W_2O_{12}$:Sm^{3+}in perfect elemental proportion [27].

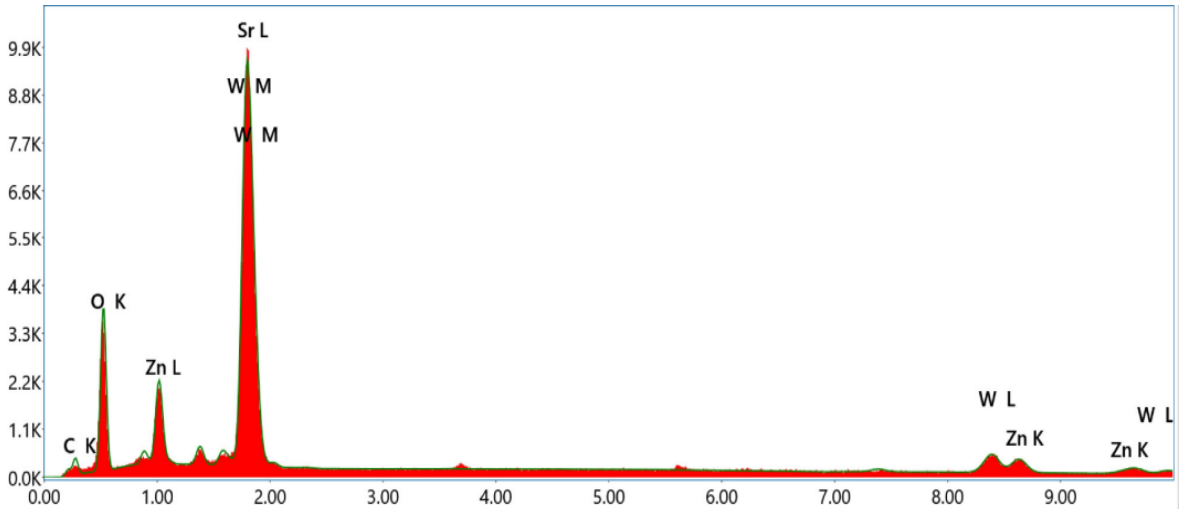

Fig.4 EDS spectrum of$Sr_4Zn_2W_2O_{12}$:xSm^{3+} (x=7 mol%) doped phosphor.

4.4. Fourier Transform Infrared Spectroscopy Analysis

FT-IR spectroscopy was utilized to investigate the internal molecular structure and identify the chemical bonding characteristics within the synthesised material by analysing its infrared absorption. Fig.5 illustrates the FT-IR spectrum of undoped $Sr_4Zn_2W_2O_{12}$ phosphor across spectral interval 400-4000 cm^{-1}. Several absorption peaks were identified by 496,697, 806,855,1071,1445,1770,2484,2878 and 2981 cm^{-1}corresponding specific vibrational modes of chemical bonds within lattice. The absorption peaks observed between 400 and 800 cm^{-1} are primarily attributed for metal-oxygen (M-O) bond stretching vibrations, confirming successful formation of the crystal lattice. Specifically, The lowest peak is at 496cm^{-1}, where the sharp bands located between 806 and 855cm^{-1} are characteristic of W-O-W stretching vibrations [28]. The peak near1071cm^{-1} represents the asymmetric stretching mode ofWO_6 octahedral units [29,30]. High-intensity peak at 1445cm^{-1} confirms the presence of Sr-O bond within the host structure [31]. Asymmetric stretching mode of C-O bonds is identified as the vibrational bond at 1770 cm^{-1}[0]. Minor peaks detected in 2878-2981cm^{-1}region indicate traces of organic impurities, associated to the asymmetric stretching of CO_2 molecules absorbed on the surface [32,33].

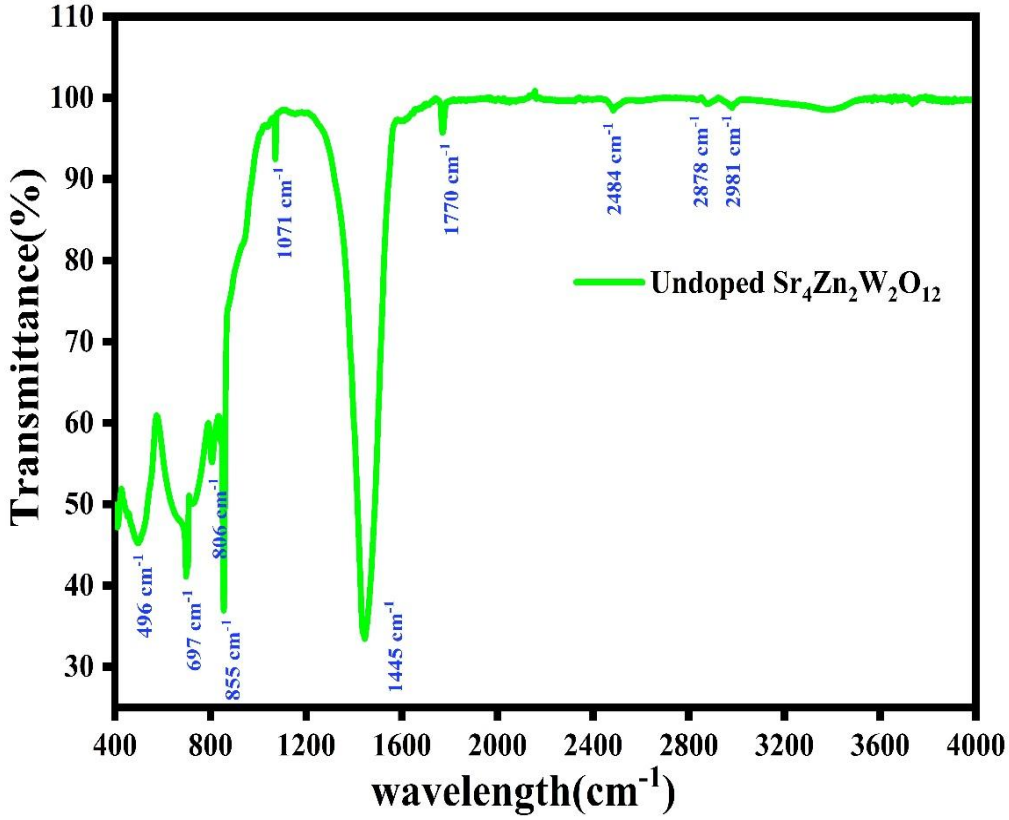

Fig.5. FT-IR spectrum of an undoped $Sr_4Zn_2WO_{12}$phosphor.

3.5. Diffuse Reflectance Spectra and Optical Band Gap Determination

DRS was used to examine the optical properties of phosphor materials because they are opaque and made in powder form. The DRS spectra of the synthetic $Sr_4Zn_2W_2O_{12}$:xSm^{3+}(x=3,5, 7 and9mol%) phosphors are displayed in Fig. 6. The spectra were recorded between200-1600 nm. Electronic excitation from lowest energy level $^6H_{15/2}$ to several high energy states $^3H_{7/2}$, $^4F_{7/2}$, $^4I_{11/2}$,$^6F_{11/2}$, $^6F_{9/2}$, $^6F_{7/2}$, $^6F_{5/2}$, $^6H_{13/2}$ and $^6H_{11/2}$are represented by the observed peaks. These transitions occur at respective wavelengths 324,408, 476,954, 1084, 1236, 1383,1488 and 1551 nm due to absorption of incident light energy.

To determine the optical band gap from the reflectance data, reflectance (R) was converted into absorption coefficient (α) using the Kubelka-Muck (K-M) function: [34]

$$F(R) = \frac{(1-R^2)}{2R} = \frac{\alpha}{S} \quad (3)$$

Where S represents the scattering coefficient. This equation allows for isolation of material's absorption characteristics. Subsequently, optical band gap (E_g) was calculated using the Tauc relations [35]:

$$\alpha hv = A(hv - E_g)^n \quad (4)$$

The Tauc equation (4), E_g represents the optical band gap energy, A is constant related to material's transition probability and hν denotes the incident photon energy. The exponent n characterizes transition type, where n=1/2 or n = 2 indicate allowed direct as well as allowed indirect transitions correspondingly. Given that Kubelka-Muck function F(R) is linearly related to absorption coefficient (α), substituted into Tauc equation as follows [36].

$$F(R) = A(hv - E_g)^n \quad (5)$$

By plotting $[F(R)hv]^{1/2}$ vs (hν) along with extrapolating linear section of resulting Tauc plot to horizontal axis, values of E_g were obtained. As shown in Fig.8, calculated band gap energies of $Sr_4Zn_2W_2O_{12}:xSm^{3+}$ (x=3,5, 7,9 mol%) are 3.74,3.72,3.71 and 3.68 eV in order. As Sm^{3+} concentration (x) rises, band gap energy is found to decrease illustrates in Fig. 7.

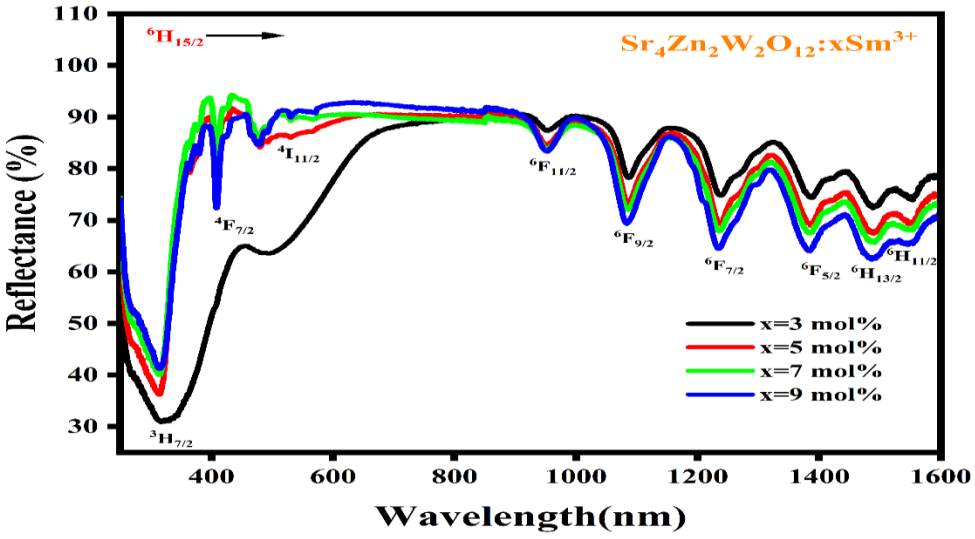

Fig.6. Diffusion reflectance spectra of $Sr_4Zn_2W_2O_{12}:xSm^{3+}$ (x=3, 5, 7 and 9 mol%) phosphors.

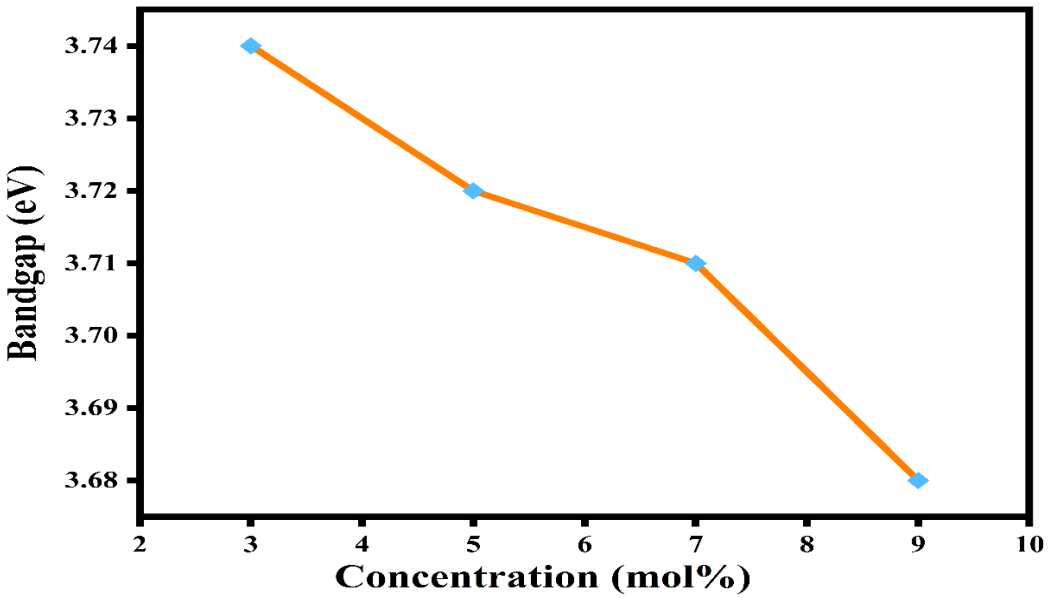

Fig.7. Variation of bandgap vs concentration.

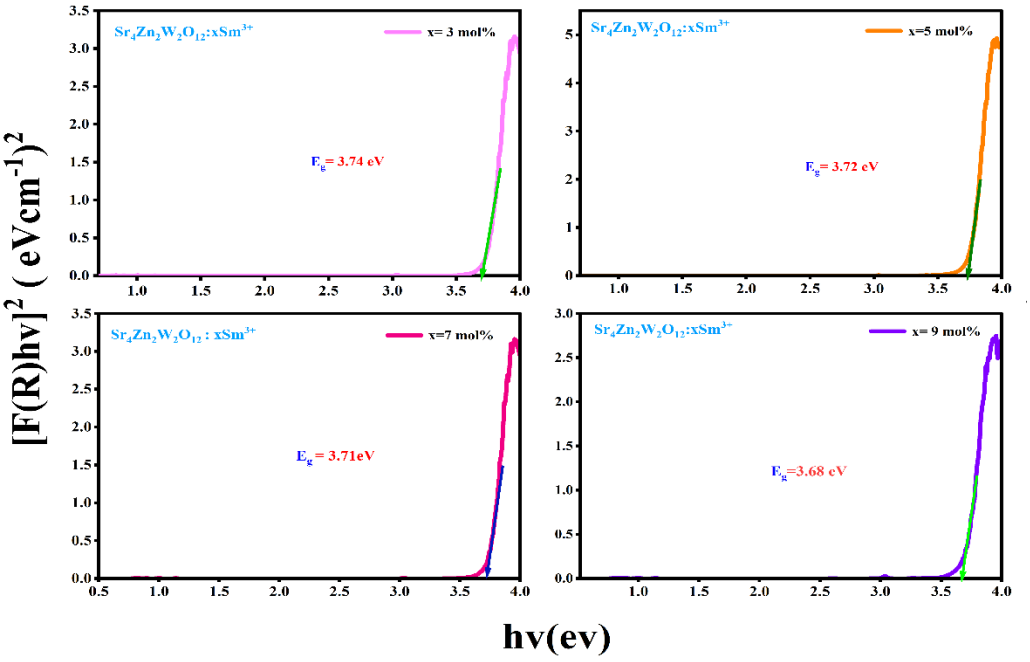

Fig.8. Tauc's plots for direct band gap of Sm^{3+} ions doped $Sr_4Zn_2W_2O_{12}$ phosphors at different concentrations.

3.6. Photoluminescence (PL) Analysis

Photoluminescence spectroscopy was used to analyse the optical characteristics of Sm^{3+}-activated $Sr_4Zn_2W_2O_{12}$ phosphors. For different Sm^{3+} concentrations (x=3, 5, 7and 9 mol%) excitation spectra were recorded in 225–500 nm region.Fig. 9 depicts PL excitation spectra of$Sr_4Zn_2W_2O_{12}$:xSm^{3+} (x=3,5, 7,9 mol%) phosphors under 645 nm emission wavelength. Ten distinct electronic transitions originating from $^6H_{5/2}$ ground state were identified. Specifically, these peaks correspond the transitions to higher energy levels $^4D_{5/2}$, $^4D_{3/2}$, $^6P_{7/2}$, $^4G_{11/2}$, $^4F_{7/2}$, $^4M_{19/2}$, $^4I_{13/2}$, $^4I_{11/2}$, $^4M_{15/2}$ and $^4I_{9/2}$. The observed excitation peaks were located at wavelengths of 347, 364, 378, 391, 406, 421, 440, 463, 480 and 491 nm respectively [37-40]. Among these, most prominent excitation peak is centred at 406 nm, which corresponds to $^6H_{5/2} \rightarrow {}^4F_{7/2}$ spectral line. The highest peak confirms that synthesised $Sr_4Zn_2W_2O_{12}$:Sm^{3+} are highly compatible with ultraviolet (UV) and near-UV radiation sources, making them suitable candidate for solid-state lighting technologies.

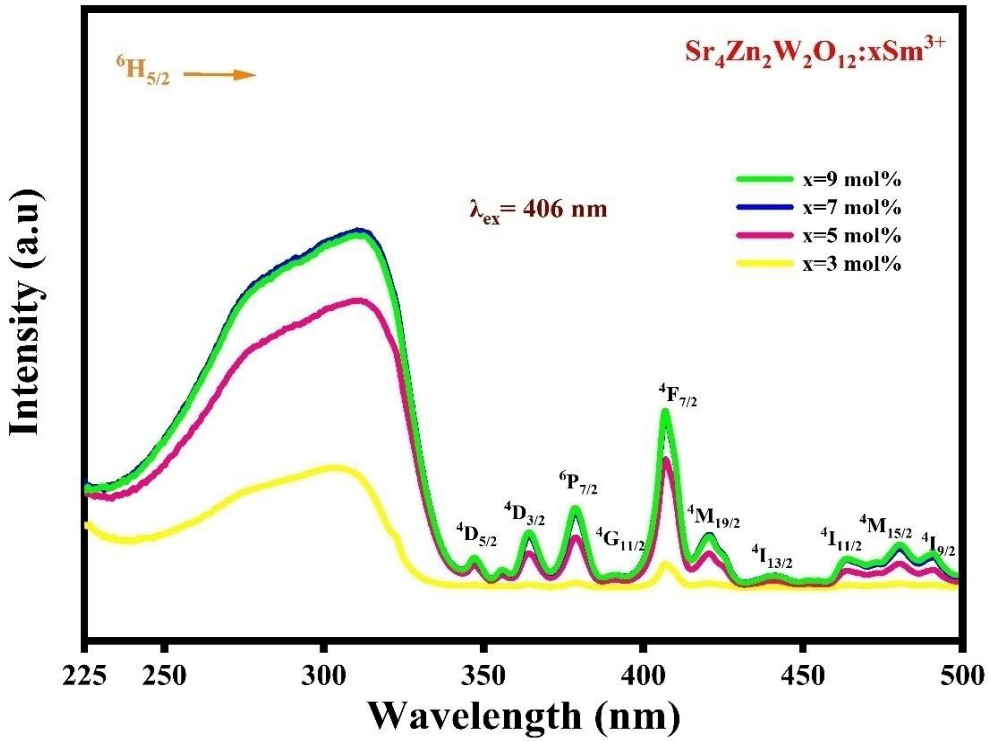

Fig.9. PL excitation spectra of $Sr_4Zn_2W_2O_{12}$:xSm^{3+} (x=3,5, 7,9 mol%) Phosphors under 645 nm emission wavelength.

Emission spectra, which illustrate radiative relaxation of electrons from excited energy levels to ground state shown, are presented in Fig. 10. Four primary emission peaks were identified at wavelengths of 536, 598, 645 and 706 nm. The corresponding 4f→4f conversion of Sm^{3+} ions is represented by these peaks: $^4G_{5/2} \rightarrow {}^6H_n$ (n= 5/2, 7/2, 9/2 and11/2) in order [64]. The dominant emission peak occurs around 645nm, originating from$^4G_{5/2} \rightarrow {}^6H_{9/2}$ transition. The transition resides within visible spectrum and produces a vivid reddish-orange luminescence. These optical characteristics demonstrate that Sm^{3+} ions effectively sensitised within the$Sr_4Zn_2W_2O_{12}$ host lattice, enabling the phosphor to serve as an efficient component for high-performance white-LED applications [41].

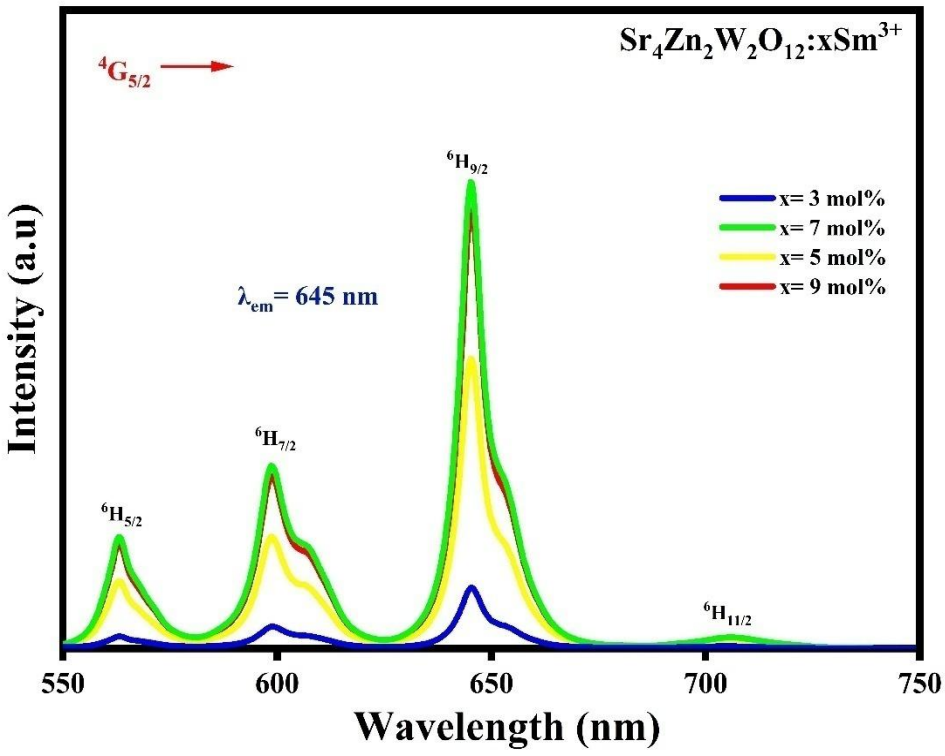

Fig.10. PL emission spectra of $Sr_4Zn_2W_2O_{12}$:xSm^{3+} (x=3,5, 7,9 mol%) Phosphors under 406 nm excitation wavelength.

The emission band centred at 645nm, originating from $^4G_{5/2} \rightarrow {}^6H_{9/2}$ peak, primarily governed by an electric doublet Mechanism ($\Delta J \leq 6$; J or J′= 0,2,4, 6). In contrast, the emission at 536 nm, corresponding to$^4G_{5/2} \rightarrow {}^6H_{5/2}$ emission, arises solely from magnetic doublet transitions (ΔJ =+1, 0,-1). The intermediate emission peak at 598nminvolves$^4G_{5/2} \rightarrow {}^6H_{7/2}$ which contributes mixed multipole transition [42]. In general, electric dipole transitions are parity-for bidden for 4f→4f electronic transitions, their relative intensity compared to magnetic dipole transitions was highly sensitive to local symmetry surrounding the optically active ion [43]. A dominant electric dipole transition indicates a highly asymmetric local environment, whereas magnetic dipole transitions are largely Independent of site symmetry. In the current$Sr_4Zn_2W_2O_{12}$ lattice, the pronounced electric dipole emission associated with the $^4G_{5/2} \rightarrow {}^6H_{9/2}$ transitions at 645nm significantly surpasses the magnetic dipole transitions, confirming that Sm^{3+}ions occupy sites with low symmetry. This highly asymmetric crystal field facilitates intense reddish-orange emission with excellent colour purity.

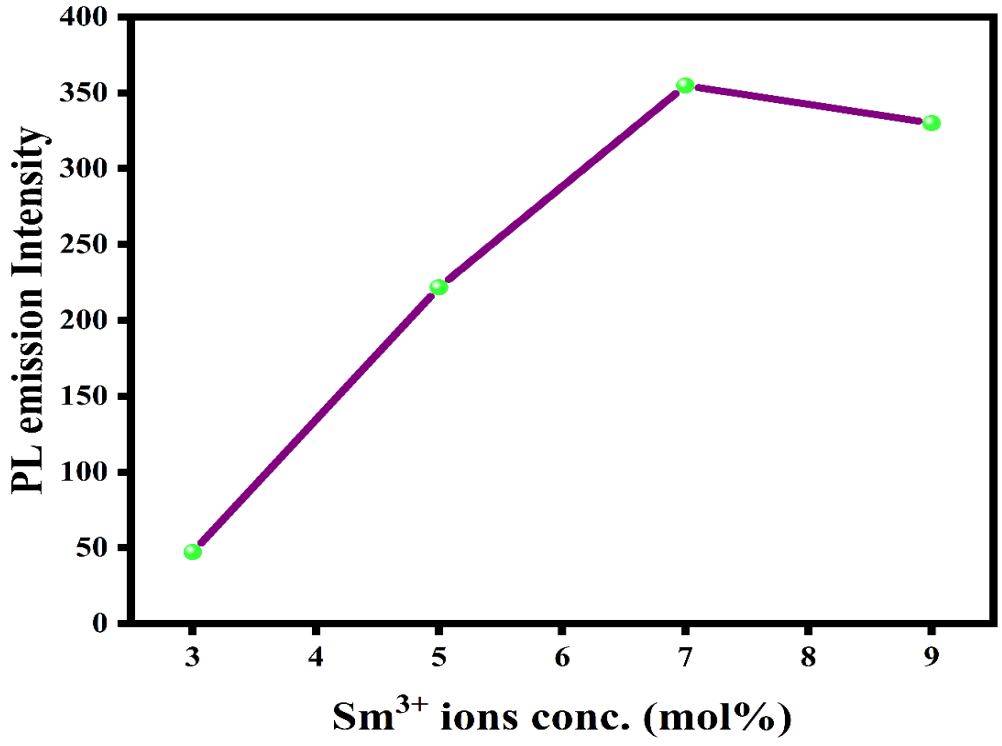

Fig.11. Variation of PL emission Intensity with Sm^{3+}ion Concentration.

The variation of photoluminescence emission intensity as a function of Sm^{3+} ion concentration was depicted in Fig. 11. The PL intensity initially increases with rising Sm^{3+}concentration, reaching a maximum at x = 7 mol%. Beyond this threshold, a subsequent decrease in intensity is observed, a phenomenon known as concentration quenching. The quenching effect was attributed by resonance energy transfer pathways within Sm^{3+} ions. Heavily doped levels, the inter-ionic distance decreases, which enhances the probability of non-radiative energy migration and effectively triggers quenching effects. Therefore, an optimal doping level of x=7mol% was identified for maximising the luminescent performance of the $Sr_4Zn_2W_2O_{12}$:Sm^{3+} phosphor system.

To Identify the specific nature of energy transfer among Sm^{3+} ions, critical distance was calculated using Blasse's equation [44]:

$$R_c \approx 2\left[\frac{3V}{4\pi X_c N}\right]^{1/3} \quad (6)$$

Here, N denotes number of available cation sites identified as 8. V is the unit cell volume determined to be 276.70 $Å^3$ and X_C is the critical Sm^{3+} concentration (x= 7mol%). The computed R_C value is 9.810Å exceeds the 5Å threshold, confirming that electric multipolar- interactions rather than exchange interactions dominant energy transfer process in these phosphors.

To further elucidates the specific multipolar interaction type, Dexter's theory was applied to evaluate the relationship between activator concentration (x) and emission Intensity (I) [45]:

$$log\left(\frac{I}{x}\right) = A - \frac{slog(x)}{d} \quad (7)$$

Inside equation, d=3 for three-dimensional compounds, A is constant and the parameter s determines the interaction type. Specifically, permanent dipole-dipole interactions are represented by s=6, dipole-quadrupole by s=8 and quadrupole-quadrupole interactions by s=10[46]. Fig. 12 revels analysis of linear fit in between log(I/x) and log(x) yieldeds = 5.1, which is closest to 6. This finding identifies dipole-dipole interactions as primary mechanism responsible for concentration quenching in the $Sr_4Zn_2W_2O_{12}$:Sm^{3+}phosphor system.

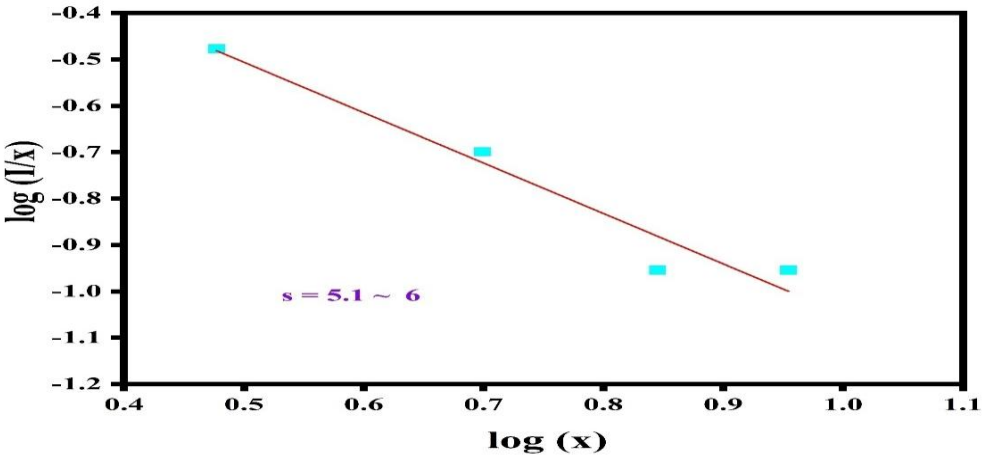

Fig.12. plot of log(I/x) vs log(x).

Fig. 13(a) illustrate various energy transfer pathways within Sm^{3+}-doped$Sr_4Zn_2W_2O_{12}$ systems and Fig.13(b) represents cross-relaxation channels (CRC) and general energy transfer (ET) processes. Upon excitation, Sm^{3+} ions are promoted to higher-energy levels, followed by rapid non-radiative relaxation to metastable $^4G_{5/2}$ state. Radiative transitions then occur out of $^4G_{5/2}$ level to lower energy levels, specifically $^6H_{5/2}$, $^6H_{7/2}$ along with $^6H_{9/2}$. For higher dopant concentrations, interactions between proximate Sm^{3+} ions promote self-quenching via non-radiative channels, which includes resonant energy transfer and cross relaxation. These mechanisms lead to a decrease in luminescence efficiency once the critical concentration is exceeded [27, 47].

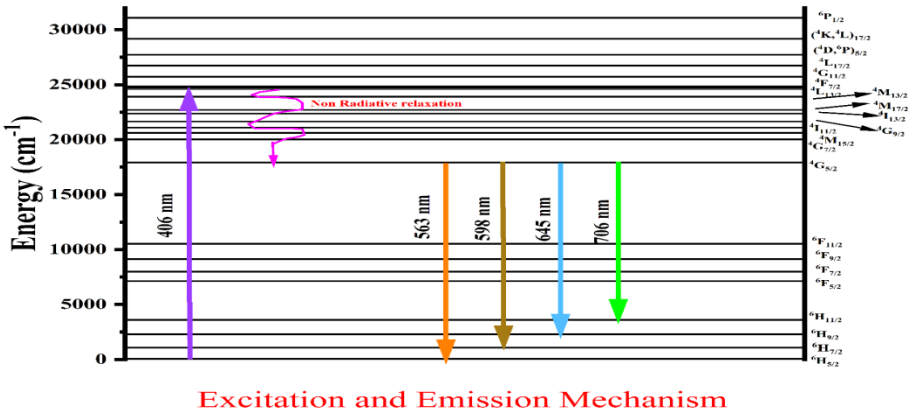

Fig.13(a) Partial energy level diagram of Sm^{3+} ion doped $Sr_4Zn_2W_2O_{12}$ phosphors.

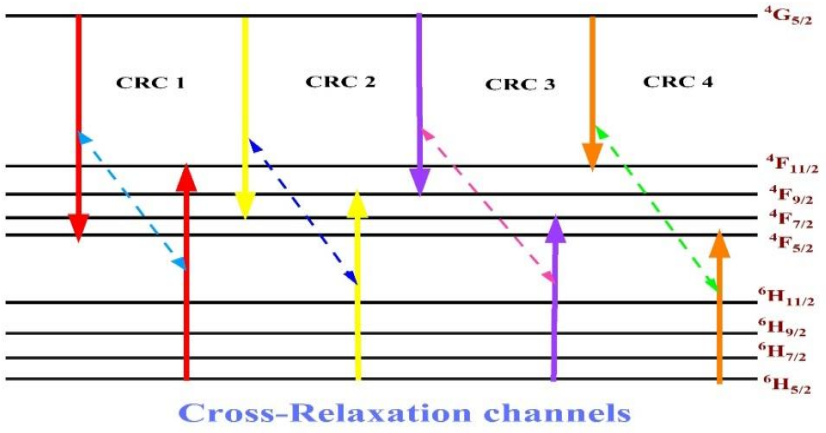

Fig.13(b). cross-relaxation channels of Sm^{3+} ions in $Sr_4Zn_2W_2O_{12}$ host lattice.

CRC 1:($^4G_{5/2} + {}^6H_{5/2} \rightarrow {}^6F_{5/2} + {}^6F_{11/2}$),

In first cross-relaxation channel, excited Sm^{3+} ion undergoes non- radiative transition from the $^4G_{5/2}$ state to $^6F_{5/2}$. The energy released in this decay is simultaneously transferred to a neighbouring ground-state, promoting it from $^6H_{5/2}$ to the $^6F_{11/2}$ level.

CRC 2:($^4G_{5/2} + {}^6H_{5/2} \rightarrow {}^6F_{7/2} + {}^6F_{9/2}$),

In second cross-relaxation channel, excited Sm^{3+} ion undergoes non- radiative transition from the $^4G_{5/2}$ state to $^6F_{7/2}$. The energy released in this decay is simultaneously transferred to a neighbouring ground-state, promoting it from $^6H_{5/2}$ to the $^6F_{9/2}$ level.

CRC 3:($^4G_{5/2} + {}^6H_{5/2} \rightarrow {}^6F_{9/2} + {}^6F_{7/2}$),

In third cross-relaxation channel, excited Sm^{3+} ion undergoes non- radiative transition from the $^4G_{5/2}$ state to $^6F_{9/2}$. The energy released in this decay is simultaneously transferred to a neighbouring ground-state, promoting it from $^6H_{5/2}$ to the $^6F_{7/2}$ level.

CRC 4:($^4G_{5/2} + {}^6H_{5/2} \rightarrow {}^6F_{11/2} + {}^6F_{5/2}$),

In fourth cross-relaxation channel, excited Sm^{3+} ion undergoes non- radiative transition from the $^4G_{5/2}$ state to $^6F_{11/2}$. The energy released in this decay is simultaneously transferred to a neighbouring ground-state, promoting it from $^6H_{5/2}$ to $^6F_{5/2}$ level.

3.7. Colorimetric Characteristics CIE and CCT Analysis

The chromatic performance of the synthesised $Sr_4Zn_2W_2O_{12}$:xSm^{3+} (x=3,5, 7,9mol%) phosphors was evaluated by determining Commission Internationale del'Eclairage (CIE) coordinates from emission data recorded under 406 nm excitation. As detailed in Table1and illustrated in Fig. 14, emission coordinates regarding all dopant concentrations are consistently localized within the reddish-orange spectral domain.

Additionally, the dominant wavelength approach was used to determine the colour purity (CP) [48]

$$Color\ Purity = \frac{\sqrt{(x-x_i)^2+(y-y_i)^2}}{\sqrt{(x_d-x_i)^2+(y_d-y_i)^2}} \quad (8)$$

Here, (x, y) stands for chromaticity coordinates of synthesized sample, (x_i, y_i) denotes equal energy point (0.333,0.333) and (x_d, y_d) is coordinates of dominant emission wavelength. According to the analysis an exceptional colour purity of 99.99% was achieved at x=7mol% Sm^{3+} concentration [0]. In contrast to phosphor lattice that was previously reported this result signifies a huge improvement. The high color purity with excitation in the near-UV spectrum, indicates $Sr_4Zn_2W_2O_{12}$:xSm^{3+} is a perfect lattice for the applications of high-quality reddish-orange emission.

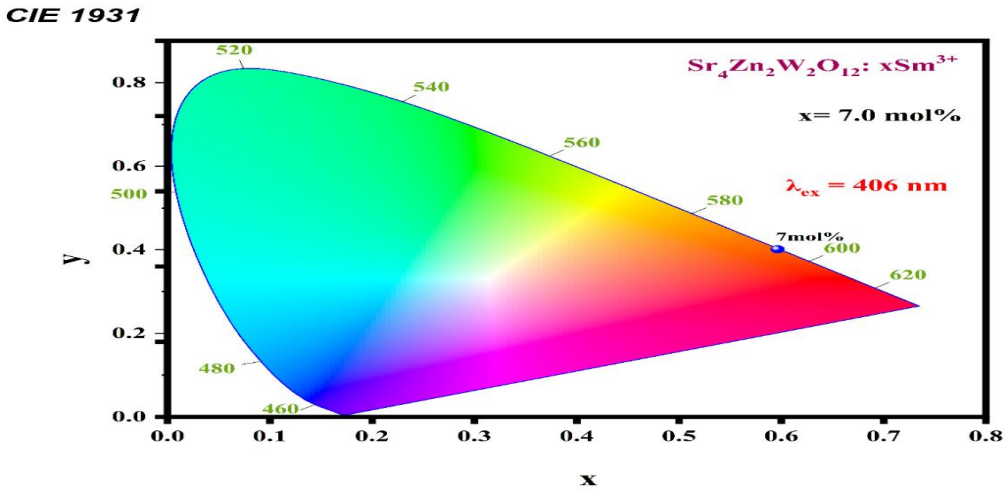

Fig.14. CIE chromaticity coordinates of $Sr_4Zn_2W_2O_{12}$:xSm^{3+}(x=7 mol%) phosphor.

To find color appearance of light source, Correlated Color Temperature (CCT) was determined. This parameter reflects the black-body temperature that mostly matches the source's chromaticity. McCamy proposed a cubic polynomial approach described as follows [24]

$$CCT = -449w^3 + 3525w^2 - 6823.20w + 5520.30 \quad (9)$$

Where w is calculated using the relationship $w = \frac{x-0.3320}{y-0.1858}$. The lower CCT values indicate warmer tones, while higher values indicates cool light [50]. The Sm^{3+}-doped $Sr_4Zn_2W_2O_{12}$ phosphors exhibits CCT values under 3000 K, highlighting their potential for warm light applications.

Table:1CIE coordinates, color purity (CP%), corelated color temperature (CCT) of $Sr_4Zn_2W_2O_{12}$:xSm^{3+}(x=3,5, 7, 9 mol%) phosphors.

Sample (mol%)	CIE coordinates		Color purity (%)	CCT (K)
	X coordinate	Y coordinate		
3	0.562	0.426	96.92	1828
5	0.591	0.404	98.97	1637
7	0.596	0.401	99.99	1625
9	0.597	0.400	99.81	1624

3.8. Time–Resolved Photoluminescence Analysis

The decay kinetics of reddish-orange emission from synthesized $Sr_4Zn_2W_2O_{12}$:xSm^{3+}(x=3,5, 7, 9 mol%) phosphors were investigated at room temperature. Analysis was conducted under excitation wavelength of 406nm, while monitoring emission peak at 645nm. To accurately described the experimental data, several decay models were evaluated; a bi-exponential decay function was found to provide the most precise fit shown in Fig. 15[51].

Emission decay behaviour is mathematically represented by the following relation [52, 53]:

$$I = I_0 + D_1 e^{-t/\tau_1} + D_2 e^{-t/\tau_2} \quad (10)$$

Wherein I denotes luminescence intensity by specific time (t), I_0 represents initial intensity at t=0. The constants D_1 and D_2 correspond to the fractional contribution of respective decay components, while τ_1 and $\tau_2$represent the individual decay lifetimes.

Furthermore, the average lifetime (τ_{avg}) of phosphor was determined using weighted expression [54-56]:

$$< \tau_{avg.} > = \frac{D_1 \tau_1^2 + D_2 \tau_2^2}{D_1 \tau_1 + D_2 \ \tau_2} \quad (11)$$

Calculated mean lifetime (τ_{avg}) values for $Sr_4Zn_2W_2O_{12}$:xSm^{3+} (x=3,5, 7,9 mol%) phosphors are 0.687, 0.622, 0.621 and 0.608 ms, exhibiting a progressive decline Sm^{3+} concentration. This trend is linked to enhanced resonance energy transfer among adjacent activator charged species. The reduction in τ_{avg} at higher doping levels confirms a higher probability of ion- ion interaction and cross-relaxation processes. Similar quenching behaviour has been documented in various rare-earth-doped oxide systems, reinforcing their suitability for solid-state lighting and optical sensing applications [57].

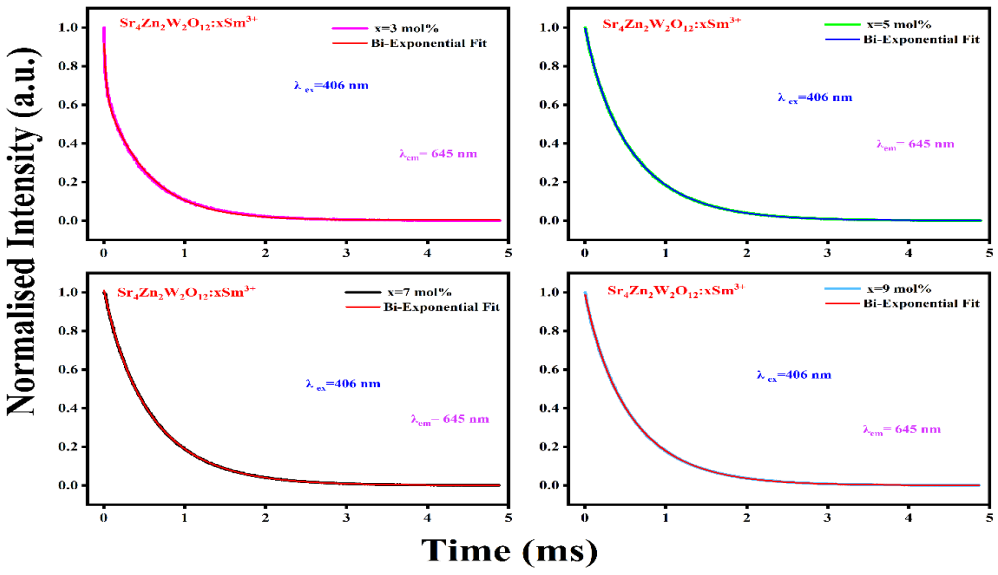

Fig.15. PL decay profiles of$Sr_4Zn_2W_2O_{12}$:xSm^{3+} (x=3,5, 7,9 mol%) phosphors.

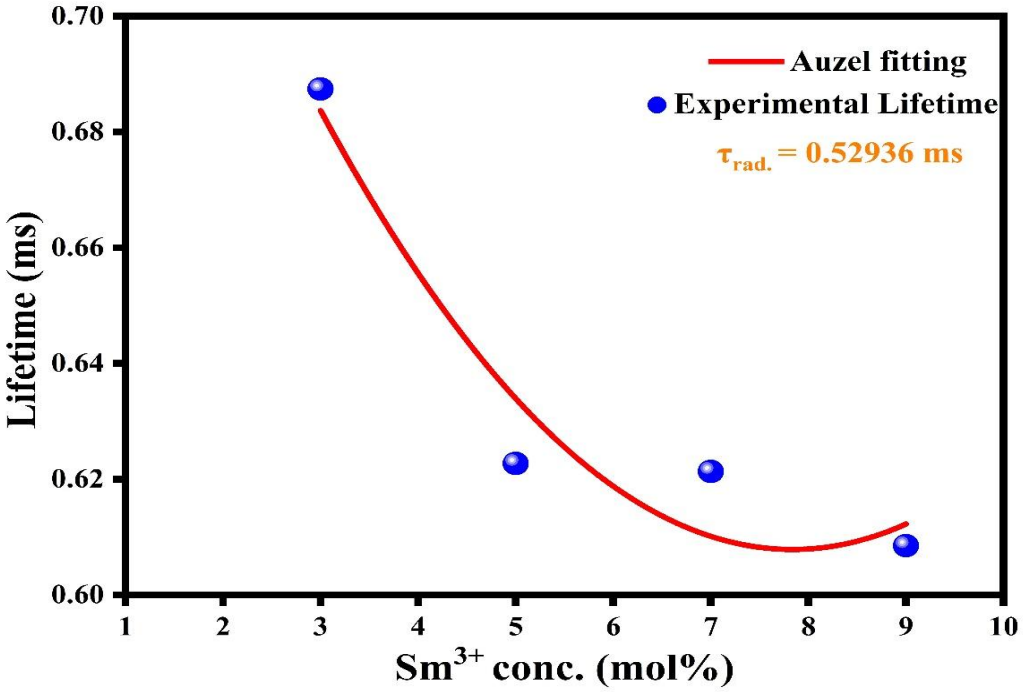

Fig.16. Auzel fitted curve illustrating the variation of decay lifetime with different concentrations of Sm^{3+}.

Fig. 16 represents reduction in decay lifetime as a function of Sm^{3+} concentration, Auzel's model was employed using the following relationship [58]:

$$\tau_{avg} = \frac{\tau_0}{1 + \frac{c}{c_0 e^{-\frac{N}{3}}}} \quad (12)$$

where c represents the Sm^{3+} dopant concentration, c_0 is a fitting constant, and N denotes number of photons involved in relaxation process. Here, τ_0 signifies intrinsic radiative lifetime. The application of Auzel's model to the $Sr_4Zn_2W_2O_{12}$:xSm^{3+} phosphor series yielded the radiative lifetime value(τ_0) to be0.806 ms.

Table 2: Decay lifetimes ($\tau_{avg,}$), radiative lifetime (τ_0), Quantum efficiency (%) and energy transfer efficiency η_{ET} for $Sr_4Zn_2W_2O_{12}$:xSm^{3+} (x=3,5, 7,9 mol%).

Sm^{3+} conc. mol (%)	**τ_{avg} (ms)**	**τ_0 (ms)**	**Quantum efficiency (%)**	**η_{ET}**
3	0.687	0.806	85.1	14.8
5	0.622	0.806	77.1	22.8
7	0.621	0.806	76.9	23.0
9	0.608	0.806	75.4	24.5

Furthermore, critical photophysical parameters, including quantum efficiency (η_{QE}) and energy-transfer efficiency (η_{ET}) were determined using stablished lifetime-based relationships [59, 60]. The internal quantum efficiency was derived from ratio of calculated average lifespan to intrinsic radiative lifetime(τ_0) [61]:

$$\text{Quantum efficiency (\%)} = \frac{\tau_{avg}}{\tau_0} \times 100 \quad (13)$$

Additionally, the energy transfer efficiency (η_{ET}), which quantifies the fraction of excitation energy exchanged via ion-ion interaction, was calculated as follows [62]:

$$\eta_{ET} = 1\text{-}\frac{\tau_{avg}}{\tau_0} \times 100 \quad (14)$$

The values of Decay lifetimes, radiative lifetime, Quantum efficiency and energy transfer efficiency η_{ET} for $Sr_4Zn_2W_2O_{12}$:xSm^{3+} (x=3,5, 7,9 mol%) are represented in Table 2.

3.9. Temperature-Dependent Photoluminescence (TDPL)

The presence of structural defects, often referred to as trap states, can lead to the loss of excitation energy through non-radiative pathways. To investigate the energy barriers associated with these defects and evaluate the thermal quenching behaviour of the material, Temperature-Dependent Photoluminescence (TDPL) analysis was performed. The TDPL spectra were recorded by monitoring emission intensity against wavelength, using an excitation wavelength of

406 nm over temperature range 50°C to 175°C as shown in Fig.17. $Sr_4Zn_2W_2O_{12}:xSm^{3+}$(x=7mol%) phosphor demonstrates significant resistance to thermal degradation. Taking the emission intensity at 50°C as 100%, a gradual decrease in luminescence is observed while temperature rises. As shown in Fig.18, the emission intensity at highest temperature of 175°C is 76.43% belonging to its original value. This intensity shows that the synthesized phosphor series achieves maximal thermal stability at a concentration of x=7 mol%.

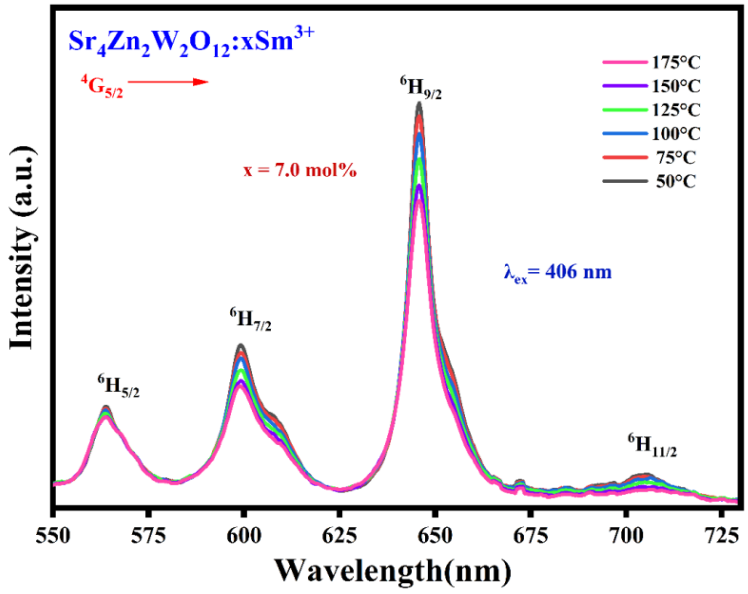

Fig.17. PL emission spectra of $Sr_4Zn_2W_2O_{12}:xSm^{3+}$ (x=3, 5, 7, 9 mol%) phosphors under 406 nm excitation wavelength.

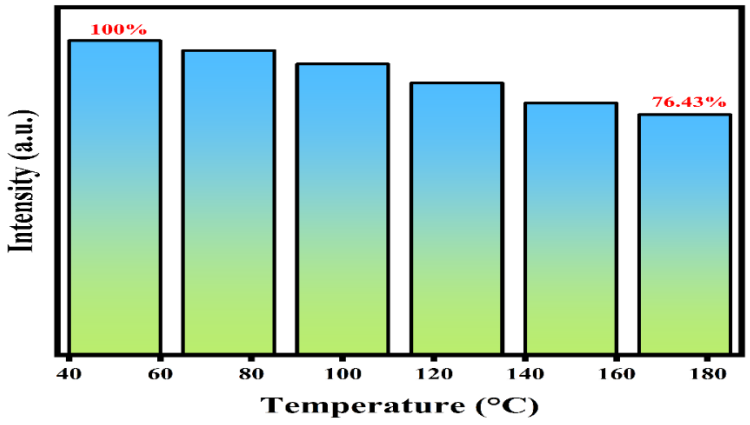

Fig.18. Bar graph of Temperature vs intensity.

The Arrhenius equation was applied to temperature-dependent emission data in order to further determine activation energy (ΔE). ΔE represents thermal energy required per carrier for escape from a trap state or luminescent center to the quenching level via non-radiative recombination. The relationship between photoluminescence (PL) intensity and temperature is expressed as follows [63].

$$I_T = \frac{I_0}{1+Cexp(\frac{-\Delta E}{K_B T})} \quad (14)$$

In this expression, I_T denotes the PL intensity at a specific absolute temperature T, I_0 represents the initial PL intensity extrapolated to 0K, A is a frequency factor or a constant related to the ratio of non-radiative to radiative recombination rates, k_B is the Boltzmann constant ($8.617*10^{-5}$eV/K). The value of ΔE was determined by line arising the Arrhenius equation and plotting $\ln[(I_0/I(T)) -1]$ vs $1/k_BT$, as depicted in Fig.19. Following a linear fit of the experimental data, R^2 value 0.983 was achieved, indicating high degree of correlation. From the slope of linear fit, activation energy ΔE for the $Sr_4Zn_2W_2O_{12}$:xSm^{3+}(x=7mol%) phosphor was calculated to 0.399 eV. Table3 illustrates CIE coordinates, color purity and activation energy of previously reported Sm^{3+} ions doped phosphors.

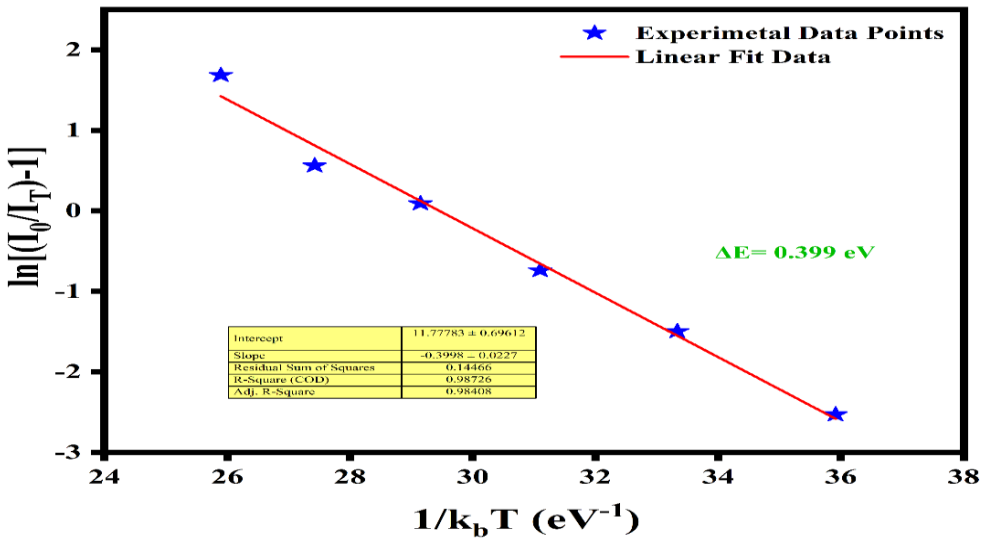

Fig.19. Linear plot of $\ln[(I_0 / I_t) -1]$ vs $1/K_BT$.

Table 3: CIE coordinates, color purity (CP%) and Activation energy of previously reported Sm^{3+} ions doped phosphors.

Host lattice	CIE coordinates		Color purity (%)	Activation energy(eV)	
	X coordinate	Y coordinate			
$Li_2Ba_5W_3O_{15}:Sm^{3+}$	0.585	0.413	88.00	0.249	
$Sr_4Ca_2W_2O_{12}:Sm^{3+}$	0.606	0.391	99.45	0.286	
$Sr_9Y_2W_2O_{24}:Sm^{3+}$	0.594	0.401	97.00	0.325	
$Sr_4Zn_2W_2O_{12}:Sm^{3+}$	0.596	0.401	99.99	0.399	This work

Chapter 5 Conclusions and scope of work

In this study, Sm^{3+}- activated tungstate-based phosphors were successfully synthesised through solid-state reaction route. A systematically characterization has been done to determine their structural, morphological, optical and luminescence properties. XRD analysis verified the generation of single-phase crystalline lattice. The calculated grain size using the Debye-Scherrer equation of $Sr_4Zn_2W_2O_{12}$:xSm^{3+}(x=0,7 mol%) are 35.39 nm and 32.47 nm, respectively. FT-IR spectroscopy verified the characteristics metal-oxygen (M-O) bonding within host framework. Electron microscopy revealed irregular, polyhedron-shaped particles with mild agglomeration and particle sizes ranging from 4-10 µm, making them suitable for LED fabrication and phosphor coating. Tauc plot analysis revealed that the optical band gap at optimised concentration x=7 mol% was 3.71 eV. From a prominent reddish-orange radiation wavelength towards 645 nm, which corresponds to$^4G_{5/2}\rightarrow{}^6H_{9/2}$ peak, photoluminescence investigates the photoexcitation peak at 406 nm, which is attributable to$^6H_{5/2}\rightarrow{}^4F_{7/2}$transition. Dexter's dipole-dipole interaction model accurately captured the quenching concentration at x=7 mol%. The CIE coordinates of optimised concentration is (0.596,0.401) with excellent colour purity of 99.99 %. The average lifetimes of $Sr_4Zn_2W_2O_{12}$:xSm^{3+} (x=3,5, 7,9 mol%) phosphor are 0.687, 0.622, 0.621and 0.608 ms described by time-resolved photoluminescence that followed a bi-exponential decay which decreased as Sm^{3+} concentration increased due to cross-relaxation processes. Additionally, TDPL investigates an activation energy of ΔE = 0.399 eV while maintaining 76.43% emission intensity at 175 °C. All of these results signify that Sm^{3+}-doped $Sr_4Zn_2W_2O_{12}$:xSm^{3+}(x=3,5, 7 and9 mol%) phosphor as the prominent host lattice for the applications of warm w-LEDs and display technologies.

WORK SCOPES:

A review of the relevant literature has been done. synthesis technique optimization. concentration optimization of the activator/sensitizer in the optimum techniques. to increase the emission intensity by co-doping different activators/sensitizers, changing the excitation wavelength, and adjusting the doping concentration to increase this usefulness of phosphor for photonic applications such as display systems.

References:

1 Prashant Dixit, Vaibhav Chauhan , S.B. Rai , Praveen C. Pandey Realization of neutral white light emission in $CaMoO_4:4Dy^{3+}$ phosphor via Sm^{3+}co-doping J. Alloys compounds 897 (2022) 162820 https://doi.org/10.1016/j.jallcom.2021.162820.

2. Shikha Verma, Labhansh Chaurasia, Sheetal Kumari, Aman P'rasad, A.S. Rao Reddish-Orange emitting thermally stable Sm^{3+} doped Sr_2LaSbO_6 phosphor for applications in w-LEDs Journal of Photochemistry and Photobiology A: Chemistry 467 (2025) 116405.

3 S. Pimputkar, J.S. Speck, S.P. Den Baars, S. Nakamura, Prospects for LED lighting, Nat. Photonics 3 (2009) 180-182 https://doi.org/10.1038/nphoton.2009.32.

4 .S. Kumari, A.S. Rao, R.K. Sinha, Structural and photoluminescence properties of Sm3+ions doped strontium yttrium tungstate phosphors for reddish-orange photonic device applications, Mater. Res. Bull. 167 (2023). 10.1016/j.materresbull.2023.112419

5 S. Kaur, A.S. Rao, M. Jayasimhadri, Spectroscopic and photoluminescence characteristics of Sm^{3+} doped calcium alumino zincate phosphor for applications in w-LED, Ceram. Int. 43 https://doi.org/10.1016/j.ceramint.2017.02.129.

6.Heena Dahiya, Mandeep Dalal, Amanvir Singh, Anju Siwach, Manju Dahiya, Sonia Nain, V.B. Taxak, S.P. Khatkar, Dinesh Kumar Spectroscopic characteristics of Eu^{3+}-activated $Ca_9Y(PO_4)_7$ nanophosphors in Judd–Ofelt framework, Science Direct, 108 (2020) 10.1016/j.solidstatesciences.2020.106341

7 V. Singh, S. Kumari, M. Seshadri, S. Kaur, A.S. Rao, Photoluminescence characteristics of Sm^{3+} activated Y_2SiO_5 orange emitting phosphors, Solid State Commun. 378 (2024) 115397. 10.1016/j.ssc.2023.115397.

8. H. Dahiya, M. Dalal, A. Singh, A. Siwach, M. Dahiya, S. Nain, V. B. Taxak, S. P. Khatkar, D. Kumar, Spectroscopic characteristics of Eu^{3+}-activated Ca9Y(PO4)7 nanophosphors in judd-ofelt framework, solid state sci. 108 (2020) 106341 10.1016/j.solidstatesciences.2020.106341.

9. S. Chen, Y. Wang, B. Zhao, B. Deng, Y. Liu, S. Chen, J. Wang, G. Wang, R. Yu, Luminescence properties of novel orange-red- emitting $Gd_2InSbO_7:Sm^{3+}$ phosphor with high color purity for W-LEDs , J. Lumin. 237 (2021) 118148 https://doi.org/10.1016/j.jlumin.2021.118148.

10. M.K. Sahu, M. Jayasimhadri, K. Jha, B. Sivaiah, A.S. Rao, D. Haranath, Synthesis and enhancement of photoluminescent properties in spherical shaped Sm^{3+}/Eu^{3+} co-doped $NaCaPO_4$ phosphor particles for w-LEDs, J. Lumin. 202 (2018) 475–483.

https://doi.org/10.1016/j.jlumin.2018.06.002.
11 Z. Zhou, N. F. Wang, N. Zhou, Z. X. He, S. Q. Liu, Y. N. Liu, Z. W. Tian, Z. Y. Mao, H.T.Hintzen, High colour purity single-phased full colour emitting white LED phosphor $Sr_2V_2O_7$:Eu^3 J. Phys. D Appl. Phys. 46 (2013) 35104. 10.1088/0022-3727/46/3/035104.

12. P. Phogat, V.B. Taxak, R.K. Malik, Crystallographic and Optical Characteristics of Ultraviolet-StimulatedDy3+-Doped $Ba_2GdV_3O_{11}$Nanorods, J. Electron. Mater. 51 (2022) 4541–4554. https://doi.org/10.1007/s11664-022-09711-7.

13. Q. Wang, Z. Mu, L. Yang, S. Zhang, D. Zhu, Y. Yang, D. Luo, F. Wu, The synthesis and the luminescence properties of $Sr_2Ga_3La_1$-xDyxGe_3O_{14}, Phys. B Condens. Matter 530 (2018) 258–263 10.1016/j.physb.2017.11.070.

14. P. Rohilla, S. Kumari, Ravita, S. Diwakar, R. Talewar, A. Shandilya, K. Maheshwari, M. Venkateswarlu, A. Prasad, A.S. Rao, Colour tuning in Sm^{3+} activated and Sm^{3+}/Eu^{3+} co-activated $SrBi_4Ti_4O_{15}$ phosphors for w-LED applications, J. Mol. Struct. 1312 (2024) 138521. 10.1016/j.molstruc.2024.138521.

15.S.B. Jiang, H. Yamamoto, M.J.F. Digonnet, J.W. Glesener, J.C. Dries, White LED phosphors: the next step, Proc. SPIE 7598 (2010) 759808. https://doi.org/10.1117/12.843536.

16. J. Zhong, M. Xu, D. Chen, G. Xiao, Z. Ji, Novel red-emitting Sr_2LaSbO_6:Eu^{3+} phosphor with enhanced $^5D_0 \rightarrow {}^7F_4$ transition for warm white light-emitting diodes, Dye. Pigment.146 (2017) 272–278. 10.1016/j.dyepig.2017.07.019.

17. N. Deopa, A.S. Rao, A. Choudhary, S. Saini, A. Navhal, M. Jayasimhadri, D. Haranath, G. Vijaya Prakash, Photoluminescence investigations on Sm^{3+} ions doped borate glasses for tricolor w-LEDs and lasers, Mater. Res. Bull. 100 (2018) 206–212. 10.1016/j.materresbull.2017.12.019.

18. L.Shi,S.Wang,Y.jieHan, Z.xinJi,D.Ma, Z. feiMu,Z. yongMao, D.jianWang, Z.wei Zhang, L. Liu, Sr_2LaSbO_6:Mn^{4+} far-red phosphor for plant cultivation: Synthesis, luminescence properties and emission enhancement by Al3+ ions, J. Lumin. 221 (2020) 6–14. https://doi.org/10.1016/j.jlumin.2020.117091.

19. G. Ouertani, M. Ferhi, K. Horchani-Naifer, M. Ferid, Effect of Sm^{3+} concentration and excitation wavelength on spectroscopic properties of $GdPO_4$:Sm^{3+} phosphor, J. Alloys Compd. 885 (2021) 161178. https://doi.org/10.1016/j.jallcom.2021.161178.

20.P. Rohilla, A.S. Rao, Synthesis optimisation and efficiency enhancement in Eu^{3+} doped barium molybdenum titanate phosphors for w-LED applications, Mater. Res. Bull. 150. 10.1016/j.materresbull.2022.111753.

21. Deepti, S. Maurya, S. Kumari, P. Rohilla, A. Prasad, A.S. Rao, Dy^{3+} doped $KCa(PO_3)_3$ phosphor for white light generation: structural and luminescent studies, Phys.Scr.99(2024). 10.1088/1402-4896/ad4def.

22. Sudarta, 済無NoTitle NoTitleNoTitle, 2022. https://doi.org/10.58355/organize.v4i3.171.

23. Bhawna, Ankita Khan, Bhabana Das, Aarti, Shailesh Narain Sharma, A.S. Rao, Synthesis, Morphology and Concentration-Dependent Photoluminescence of Thermally Stable Dy^{3+} Activated Phosphor for White LED Applications, Journal of Fluorescence 36 (2026) 1215–1228 https://doi.org/10.1007/s10895-025-04626-y

24.Anu, A.S. Rao, Temperature sensing materials based on the fluorescence intensity ratio in $Li_2Ba_5W_3O_{15}:Dy^{3+}$ phosphors, Sensors and Actuators A: Physical 372 (2024) 115336, https://doi.org/10.1016/j.sna.2024.115336.

25.Sumandeep Kaur, A.S. Rao, M. Jayasimhadri, Spectroscopic and photoluminescence characteristics of Sm^{3+} doped calcium aluminozincate phosphor for applications in w-LED, Ceramics International 43 (2017) 7401–7407, https://doi.org/10.1016/j.ceramint.2017.02.129.

26.Lei Shi, Ya-jie Han, Hui-xin Wang, Dan-chen Shi, Xiao-yu Geng, Zhi-wei Zhang, High efficiency and thermally stable far-red emission of Mn^{4+} in double cubic perovskite $Sr_9Y_2W_4O_{24}$ for plant cultivation, Journal of Luminescence 208 (2019) 307–312,https://doi.org/10.1016/j.jlumin.2018.12.065.

27. Kanika Kardam, A.S. Rao, R.K.Sinha, Study on the luminescence and structural properties of the novel $Sr_4Ca_2W_2O_{12}$ phosphors doped with Sm^{3+} for high color purity in white LED applications, Journal of Luminescence 286 (2025)121351, https://doi.org/10.1016/j.jlumin.2025.121351.

28.Ting Yang, Qirui Xiang, Li Feng, Chengli Dong, Xinru Zhang, Zhanglei Ning, Xin Lai, Daojiang Gao, Yttrium-based metal-organic frameworks: Controllable synthesis, growth mechanism and the phase transformation to $Y_2O_3:Eu^{3+}$ phosphors, Journal of Luminescence 214 (2019) 116567, https://doi.org/10.1016/j.jlumin.2019.116567.

29.N. Prabhu, S. Agilan, N. Muthukumarasamy, T.S. Senthil, Enhanced photovoltaic performance of WO_3 nanoparticles added dye sensitized solar cells, Journal of Materials Science: Materials in Electronics 25 (2014) 5288–5295,https://doi.org/10.1007/s10854-014-2303-6.

30.Vishal Chaudhary, Amarjeet Kaur, Enhanced room temperature sulfur dioxide sensing behaviour of in situ polymerized polyaniline-tungsten oxide nanocomposite possessing honeycomb morphology, RSC Advances 5 (2015) 73535–73544,https://doi.org/10.1039/C5RA08275G.

31.V. Dubey, J. Kaur, S. Agrawal, Effect of europium doping levels on photoluminescence and thermoluminescence of strontium yttrium oxide phosphor, Materials Science in Semiconductor Processing 31 (2015) 27–37,https://doi.org/10.1016/j.mssp.2014.10.052.

32.Chandni Kumari, J. Manam, S.K. Sharma, Synthesis and luminescence properties of a bluish-green -emitting Sr_3LiSbO_6: Pr^{3+} phosphor for optoelectronic applications, Ceramics International 50 (2024) 10535–10550,https://doi.org/10.1016/j.ceramint.2023.12.365.

33.Ivana Cavoski, Valeria D'Orazio, Teodoro Miano, Interactions between rotenone and humic acids by means of FT-IR and fluorescence spectroscopies, Analytical and Bioanalytical Chemistry 395 (2009) 1145–1158, https://doi.org/10.1007/s00216-009-3026-z.

34.Priya Phogat, S.P. khatkar, V.B. Taxak, R.K. Malik, Sm^{3+} doped $Bi_4MgO_4(PO_4)_2$:crystal and optoelectronic investigation of the solution combustion derived bright orange emanating novel nanophosphor for SSLs, Materials Chemistry and Physics 276 (2022) 125389, https://doi.org/10.1016/j.matchemphys.2021.125389.

35.Lili Wang, Hyeon Mi Noh, Byung Kee Moon, Sung Heum Park, Kwang Ho Kim, Jinsheng Shi, Jung Hyun Jeong, Dual-Mode Luminescence with Broad Near UV and Blue Excitation Band from Sr_2CaMoO_6:Sm^{3+} Phosphor for White LEDs, Journal of Physical Chemistry C 119 (2015) 15517–15525,https://doi.org/10.1021/acs.jpcc.5b02828.

36.Pooja Rohilla, A.S. Rao, Synthesis optimisation and efficiency enhancement in Eu^{3+} doped barium molybdenum titanate phosphors for w-LED applications, Materials Research Bulletin 150(2022) 111753, https://doi.org/10.1016/j.materresbull.2022.111753.

37.Ch.B. Annapurna Devi, K. Swapna, Sk Mahamuda, M. Venkateswarlu, M.V.V.K.S. Prasad, K. Siva Rama Krishna Reddy, Nisha Deopa, A.S. Rao, Spectroscopic studies and lasing potentialities of Sm^{3+} ions doped single alkali and mixed alkali fluoro tungstentellurite glasses, Optics and Laser Technology 111 (2019) 176–183,https://doi.org/10.1016/j.optlastec.2018.09.051.

38.Bingjie Han, Jing Ren, Ping Ping Teng, JiaBao Zhu, Yu Shen, ZhiAng Li, Xiaoliang Zhu, Xinghua Yang, Synthesis and photoluminescence properties of a novel double perovskite $Ca_2LaSbO_6:Sm^{3+}$ phosphor for w-LEDs, Ceramics International 48 (2022) 971–980,https://doi.org/10.1016/j.ceramint.2021.09.182.

39.Nisha Deopa, Sumandeep Kaur, Aman Prasad, Bipin Joshi, A.S. Rao, Spectral studies of Eu^{3+} doped lithium lead alumino borate glasses for visible photonic applications, Optics and Laser Technology 108 (2018) 434–440, https://doi.org/10.1016/j.optlastec.2018.07.010.

40.P. Shahab Khan, B.C. Jamalaiah, M. Jayasimhadri, Harpreet Kaur, N. Madhu, P. Raghupathi, K. Pavani, Deep reddish-orange emitting $Sr_3Gd(PO_4)_3$: Sm^{3+} phosphors via modified citrate-gel combustion method, Journal of Molecular Structure 1255 (2022)132428, https://doi.org/10.1016/j.molstruc.2022.132428.

41.Kirti Nanda, R.S. Kundu, Inder Pal, R. Punia, N. Kishore, Concentration dependence of intensity parameters and radiative properties of Sm^{3+} ions doped in BaO -ZnO-B_2O_3 glasses, Journal of Alloys and Compounds 676 (2016) 521–526,https://doi.org/10.1016/j.jallcom.2016.03.112.

42.Ishant Kumar, Arvind K. Gathania, Photoluminescence and quenching study of the Sm^{3+}-doped $LiBaPO_4$ phosphor, Journal of Materials Sciences: Materials in Electronics 33 (2022) 328–341, https://doi.org/10.1007/s10854-021-07301-7.

43.Ruijin Yu, Yue Guo, Lili Wang, Hyeon Mi Noh, Byung Kee Moon, Byung Chun Choi, Jung Hyun Jeong, Characterizations and optical properties of orange-red emitting Sm^{3+}-doped Y_6WO_{12} phosphors, Journal of Luminescence 155 (2014) 317–321,https://doi.org/10.1016/j.jlumin.2014.06.041.

44.Shigao Chen, Yu Wang, Baokui Zhao, Bin Deng, Yuanyuan Liu, Shansh an Chen, Jianxu Wang, Guodong Wang, Ruijin Yu, Luminescence properties of novel orange-red-emitting Gd_2InSbO_7 : Sm^{3+} phosphor with high color purity for W-LEDs, Journal of Luminescence 237 (2021) 118148,https://doi.org/10.1016/j.jlumin.2021.118148

45.Jihuan Xie, Liqun Cheng, He Tang, Xiaofang Yu, Zhongxue Wang, Xiaoyun Mi, Quansheng Liu, Xiyan Zhang, Synthesis and photoluminescence properties of NUV-excited $NaBi(MoO_4)_2$: Sm^{3+} phosphors for white light emitting diodes, Optics and Laser Technology 147 (2022) 107659,https://doi.org/10.1016/j.optlastec.2021.107659.

46.Peng Du, Xiaoyong Huang, Jae Su Yu, Facile synthesis of bifunctional Eu^{3+}-activated $NaBiF_4$ red-emitting nanoparticles for simultaneous white light-emitting diodes and field emission displays, Chemical Engineering Journal 337 (2018) 91–100,https://doi.org/10.1016/j.cej.2017.12.063.

47.G. Ouertani, M. Ferhi, K. Horchani-Naifer, M. Ferid, Effect of Sm^{3+} concentration and excitation wavelength on spectroscopic properties of $GdPO_4$:Sm^{3+} phosphor, Journal of Alloys and Compounds 885 (2021) 161178,https://doi.org/10.1016/j.jallcom.2021.161178.

48.Prashant Dixit, Vaibhav Chauhan, S.B. Rai, Praveen C. Pandey, Realization of neutral white light emission in $CaMoO_4$:$4Dy^{3+}$ phosphor via Sm^{3+} co-doping, Journal of Alloys and Compounds 897 (2022) 162820, https://doi.org/10.1016/j.jallcom.2021.162820.

49.Ji Zhao, Shan-Xiu Huang, Dan Zhao, Cun-Han Huang, Ming-Jie Ma, Rui-Juan Zhang, Yun-Chang Fan, Bao-Zhong Liu, Jia-Wang Gao, Qiu Zong, Ya-Ping Yu, Sm^{3+} doped $K_3Gd_3B_4O_{12}$: An orange-emitting phosphor for white light-emitting diodes, Optik 159 (2018) 115–122,https://doi.org/10.1016/j.ijleo.2018.01.043.

50.Ravina Lohan, A. Kumar, Mukesh K. Sahu, Anu Mor, V. Kumar, Nisha Deopa, A.S. Rao, Structural, thermal, and luminescence kinetics of $Sr_4Nb_2O_9$ phosphor doped with Dy^{3+} ions for cool w-LED applications, Journal of Materials Science: Materials in Electronics 34 (2023) 694,https://doi.org/10.1007/s10854-023-10055-z.

51.Bhawna, Shailesh Narain Sharma, A.S. Rao, Up-conversion and power dependent photoluminescence studies of green emitting Er^{3+}-activated niobate phosphor for white LED

applications. Journal of Alloys and Compounds 1040 (2025) 183589https://doi.org/10.1016/j.jallcom.2025.183589.

52.Anu, A.S. Rao, Novel Orange-red-emitting $Li_2Ba_5(WO_5)_3:Eu^{3+}$ phosphor for wLEDs and non-contact thermometry applications, Journal of Materials Science: Materials in Electronics 34 (2023) 2191, https://doi.org/10.1007/s10854-023-11602-4.

53.P.Rekha Rani, M. Venkateswarlu, K. Swapna, Sk. Mahamuda, M.V.V. K. Srinivas Prasad, A.S. Rao, Spectroscopic and luminescence properties of Ho^{3+} ions doped barium lead alumino fluoro borate glasses for Green laser applications, Solid State Sciences 102 (2020) 106175, https://doi.org/10.1016/j.solidstatesciences.2020.106175.

54.Anu, A.S. Rao, Luminescence and optical thermometry strategy based on emission spectra of $Li_2Ba_5W_3O_{15}:Pr^{3+}$ phosphors, Optical Materials 145 (2023) 114476. https://doi.org/10.1016/j.optmat.2023.114476.

55.Anu, Seema, A. Kumar, Nisha Deopa, Mukesh K. Sahu, Aman Prasad, A.S. Rao, A single phase $Li_2Ba_5W_3O_{15}:Dy^{3+}/Eu^{3+}$ phosphor for color tunable devices and non-contact optical thermometry, Journal of Luminescence 269 (2024) 120444, https://doi.org/10.1016/j.jlumin.2024.120444.

56.Ravina, Kanishk Poria, Mukesh K. Sahu, A. Kumar, Anu, Sajjan Dahiya, Nisha Deopa, A.S. Rao, Energy transfer mechanisms and color-tunable luminescence of $Tm^{3+}/Tb^{3+}/Eu^{3+}$ codoped $Sr_4Nb_2O_9$ phosphors for high-quality White light-emitting diodes, RSC Advances 13 (2023) 33675–33687, https://doi.org/10.1039/D3RA05519A.

57.Xingyang Peng, Ruirui Cui, Xiang Guo, Xingyong Gong, Jun Zhang, Chaoyong Deng, Er^{3+} activated $BaLaGaO_4$ multifunctional Green phosphors for optical thermometers and WLEDs, Journal of Rare Earths 43 (2025) 2077-2089, https://doi.org/10.1016/j.jre.2024.09.001.

58.Gaurank Yadav, Jatin Parashar, Anu, Aman Prasad, A.S. Rao, Synthesis, structural and photoluminescence characteristics of Dy^{3+}/Eu^{3+} co-doped $CaGdSbWO_8$ phosphor for warm White LEDs, Emergent Materials8 (2025) 793-809https://doi.org/10.1007/s42247-024-00960-2.

59.C. Madhukar Reddy, B. Deva Prasad Raju, N. John Sushma, N.S. Dhoble, S. J. Dhoble, A review on optical and photoluminescence studies of RE^{3+} (RE=Sm, Dy, Eu, Tb and Nd) ions doped LCZSFB glasses, Renewable and Sustainable Energy reviews 51 (2015) 566–584, https://doi.org/10.1016/j.rser.2015.06.025.

60.E. Kaewnuam, N. Wantana, H.J. Kim, J. Kaewkhao, Development of lithium yttrium borate glass doped with Dy^{3+} for laser medium, W-LEDs and scintillation materials applications, Journal of Non-Crystalline Solids 464 (2017) 96–103,https://doi.org/10.1016/j.jnoncrysol.2017.03.027.

61.Aarti, AS Rao, Shailesh Narain Sharma, Structural and photoluminescence studies of Eu^{3+}-doped $Bi_6Ti_3WO_{18}$ phosphors for solid-state lighting and optical thermometry,Journal of material science: Materials in electronics ,37,2026,514, https://doi.org/10.1007/s10854-026-16679-1 .

62.Kanika Kardam, A.S. Rao, R.K. Sinha, Investigations on luminescent properties of thermally stable Eu^{3+} doped $Sr_4Ca_2W_2O_{12}$ phosphor for high color purity in white LEDs and non-contact optical thermometry applications, Physica B: Condensed Matter,727,2026,418319,https://doi.org/10.1016/j.physb.2026.418319.

63.Pooja Rohilla, A.S. Rao, Energy transfer induced colour tunable photoluminescence performance of thermally stable Sm^{3+}/Eu^{3+} co-doped Ba_3MoTiO_8 phosphors for white LED applications, Journal of Materials Science: Materials in Electronics 34 (2023) 1662,https://doi.org/10.1007/s10854-023-11025-1.

64.Lixia Zhang, Junzhi Che, Yingying Ma, Jianxu Wang, Ruyi Kang, Bin Deng, Ruijin Yu, Huiling Geng, Luminescent and thermal properties of novel orange-red emitting $Ca_2MgTeO_6:Sm^{3+}$ phosphors for white LEDs, Journal of Luminescence 225 (2020) 117374, https://doi.org/10.1016/j.jlumin.2020.117374.

PLAGIARISM REPORT

Thesis plag report.docx

Indian Institute of Technology Jodhpur

Document Details

Submission ID
trn:oid:::29334:140619412

Submission Date
May 27, 2026, 11:42 AM GMT+5:30

Download Date
May 27, 2026, 11:49 AM GMT+5:30

File Name
Thesis plag report.docx

File Size
67.8 KB

25 Pages

6,865 Words

42,607 Characters

10% Overall Similarity

The combined total of all matches, including overlapping sources, for each database.

Filtered from the Report

- Bibliography
- Quoted Text
- Cited Text
- Small Matches (less than 8 words)

Match Groups

48 Not Cited or Quoted 10%
Matches with neither in-text citation nor quotation marks

0 Missing Quotations 0%
Matches that are still very similar to source material

0 Missing Citation 0%
Matches that have quotation marks, but no in-text citation

0 Cited and Quoted 0%
Matches with in-text citation present, but no quotation marks

Top Sources

7% Internet sources
7% Publications
6% Submitted works (Student Papers)

Integrity Flags

1 Integrity Flag for Review

Replaced Characters
6 suspect characters on 3 pages
Letters are swapped with similar characters from another alphabet.

Our system's algorithms look deeply at a document for any inconsistencies that would set it apart from a normal submission. If we notice something strange, we flag it for you to review.

A Flag is not necessarily an indicator of a problem. However, we'd recommend you focus your attention there for further review.

Match Groups

- **48** Not Cited or Quoted 10%
  Matches with neither in-text citation nor quotation marks
- **0** Missing Quotations 0%
  Matches that are still very similar to source material
- **0** Missing Citation 0%
  Matches that have quotation marks, but no in-text citation
- **0** Cited and Quoted 0%
  Matches with in-text citation present, but no quotation marks

Top Sources

7% Internet sources
7% Publications
6% Submitted works (Student Papers)

Top Sources

The sources with the highest number of matches within the submission. Overlapping sources will not be displayed.

1	Internet	
www.infrastructureontario.ca		1%
2	Internet	
ijomam.com		<1%
3	Internet	
www.mdpi.com		<1%
4	Publication	
G.B. Mahesha, B.R. Radha Krushna, M. Gagana, S.C. Sharma et al. "Multifunctional...		<1%
5	Publication	
P.Lakshmi Tirupatamma, Sk. Mahamuda, K. Swapna, M. Venkateswarlu, A.S. Rao. ...		<1%
6	Publication	
Asif Ali Haider, Jiayi He, Hongming Jiang, Asad Ullah, Wei Qian, Dandan Gao, Zhi X...		<1%
7	Internet	
ir.niist.res.in:8080		<1%
8	Internet	
research.leedstrinity.ac.uk		<1%
9	Internet	
coek.info		<1%
10	Submitted works	
Universiti Teknologi Malaysia on 2016-01-11		<1%

11	Internet	
www.science.gov		<1%
12	Submitted works	
Indian Institute of Engineering Science and Technology on 2022-02-21		<1%
13	Internet	
www2.mdpi.com		<1%
14	Submitted works	
Pukyong National University on 2016-04-20		<1%
15	Publication	
Sk. Faruque Ahmed, Geon-Ho Rho, Kwang-Ryeol Lee, Ashkan Vaziri, Myoung-Woo...		<1%
16	Submitted works	
Universiti Teknologi Malaysia on 2017-01-26		<1%
17	Publication	
Chua, Bee Bee. "Predicting Open Source Forked Pattern Survivability", University ...		<1%
18	Submitted works	
University of Wollongong on 2003-08-17		<1%
19	Internet	
doc.edu.vn		<1%
20	Internet	
hdl.handle.net		<1%
21	Internet	
usermanual.wiki		<1%
22	Submitted works	
Delhi Technological University on 2019-01-31		<1%
23	Internet	
www.nairjc.com		<1%
24	Submitted works	
Doctor Harisingh Gour Vishwavidyalaya, Sagar on 2014-07-30		<1%

25	Submitted works	
Jawaharlal Nehru Technological University Anantapur on 2014-07-08		<1%
26	Submitted works	
Kyungpook National University on 2018-01-09		<1%
27	Publication	
Linlin Gu, Mingnv Guo, Jiang He, Zhongqing Yang. "Experimental study on hydrog...		<1%
28	Publication	
P. R. Biju, Gijo Jose, P. V. Jyothy, Vinoy Thomas, N. V. Unnikrishnan. " Upconversio...		<1%
29	Publication	
Sanja Ćulubrk, Željka Antić, Milena Marinović-Cincović, Phillip S. Ahrenkiel, Mirosl...		<1%
30	Publication	
M.E. Alvarez-Ramos. "Luminescence and study of channels for cross-relaxation de...		<1%
31	Submitted works	
Universiti Putra Malaysia on 2024-08-06		<1%
32	Publication	
Xiao-Fei Wu, Jing-Jing Zhang, Ming-Fei Li, Jing Bian, Feng Peng. "Catalytic hydroth...		<1%
33	Internet	
datapdf.com		<1%
34	Internet	
etd.uovs.ac.za		<1%
35	Internet	
pdfs.semanticscholar.org		<1%

Thesis plag report.docx

Indian Institute of Technology Jodhpur

Document Details

Submission ID
trn:oid:::29334:140619412

Submission Date
May 27, 2026, 11:42 AM GMT+5:30

Download Date
May 27, 2026, 11:51 AM GMT+5:30

File Name
Thesis plag report.docx

File Size
67.8 KB

25 Pages
6,865 Words
42,607 Characters

*% detected as AI

AI detection includes the possibility of false positives. Although some text in this submission is likely AI generated, scores below the 20% threshold are not surfaced because they have a higher likelihood of false positives.

Caution: Review required.

It is essential to understand the limitations of AI detection before making decisions about a student's work. We encourage you to learn more about Turnitin's AI detection capabilities before using the tool.

Disclaimer
Our AI writing assessment is designed to help educators identify text that might be prepared by a generative AI tool. Our AI writing assessment may not always be accurate (i.e., our AI models may produce either false positive results or false negative results), so it should not be used as the sole basis for adverse actions against a student. It takes further scrutiny and human judgment in conjunction with an organization's application of its specific academic policies to determine whether any academic misconduct has occurred.

Frequently Asked Questions

How should I interpret Turnitin's AI writing percentage and false positives?
The percentage shown in the AI writing report is the amount of qualifying text within the submission that Turnitin's AI writing detection model determines was either likely AI-generated text from a large-language model or likely AI-generated text that was likely revised using an AI paraphrase tool or word spinner.

False positives (incorrectly flagging human-written text as AI-generated) are a possibility in AI models.

AI detection scores under 20%, which we do not surface in new reports, have a higher likelihood of false positives. To reduce the likelihood of misinterpretation, no score or highlights are attributed and are indicated with an asterisk in the report (*%).

The AI writing percentage should not be the sole basis to determine whether misconduct has occurred. The reviewer/instructor should use the percentage as a means to start a formative conversation with their student and/or use it to examine the submitted assignment in accordance with their school's policies.

What does 'qualifying text' mean?
Our model only processes qualifying text in the form of long-form writing. Long-form writing means individual sentences contained in paragraphs that make up a longer piece of written work, such as an essay, a dissertation, or an article, etc. Qualifying text that has been determined to be likely AI-generated will be highlighted in cyan in the submission, and likely AI-generated and then likely AI-paraphrased will be highlighted purple.

Non-qualifying text, such as bullet points, annotated bibliographies, etc., will not be processed and can create disparity between the submission highlights and the percentage shown.

PROOF OF JOURNAL PUBLICATION

Novel Thermally-Stable Sr4Zn2W2O12: Sm3+ Phosphors: Synthesis, Optical Properties and Applications in WLEDs

--Manuscript Draft--

Manuscript Number:	
Article Type:	Full Length Article
Keywords:	Photoluminescence; phosphors; w-LEDs; activation energy
Corresponding Author:	Srinivasa Rao Allam Delhi Technological University New Delhi, New Delhi INDIA
First Author:	Jaya Chandra, Msc
Order of Authors:	Jaya Chandra, Msc
	Tanya Dang, Msc
	Kanika Kardam, Ph.D
	Sheetal Kumari, Ph.D
	Srinivasa Rao Allam, Ph.D
	Shailesh Narain Sharma, Ph.D
Abstract:	A series of reddish-orange emitting Sm3+ doped phosphors based strontium zinc tungstate Sr4Zn2W2O12:xSm3+ (x=3, 5, 7 and 9 mol%) host were successfully synthesised via solid state reaction route. XRD analysis confirmed synthesis of highly crystalline lattice, indicating that dopant ions were successfully integrated into tungstate host lattice matching with standard JCPDS card no.96-156-3084. Scanning electron microscopy along with Fourier transform infrared spectroscopy characterizations provide insights into the micro structural irregular polyhedron morphology and used for identifying chemical bonds respectively. The optical band gap of Sr4Zn2W2O12 phosphors at optimize concentration x=7mol% was identified to be Eg=3.71 eV through diffuse reflectance spectroscopy (DRS). Optical investigation via photoluminescence (PL) studies a prominent excitation peak at 406 nm, under this excitation the phosphor exhibits a highly pure reddish-orange radiation recorded at 645 nm showing 4G5/2→6H9/2 energy transfer. At an optimal doping level, x=7 mol% concentration quenching phenomenon identified. The optimized phosphor showed CIE chromaticity coordinates (0.596, 0.401) along with outstanding colour purity of 99.99% and correlated color temperature (CCT) of 1625K thus making it suitable for reddish-orange emission This optimized material exhibited exceptional color purity of 99.99%, correlated color temperature (CCT) of 1625 K and CIE chromaticity coordinates (0.596, 0.401), making it appropriate for reddish-orange emission. Temperature-Dependent Photoluminescence (TDPL) results highlighted the materials robust thermal stability with retaining 76.43% emission intensity at 175oC, activation energy to be ΔE= 0.399 eV and quantum efficiency to be 76.9%. The results suggesting that Sr4Zn2W2O12:xSm3+ is a superior host for developing high performance w-LEDs.

WILEY

Dear Miss Tanya Dang,

We are pleased to inform you that the manuscript "Novel Thermally-Stable Sr4Zn2W2O12: Sm3+ Phosphors: Synthesis, Optical ,Luminescence properties and Applications in WLEDs" has been submitted to ChemistrySelect by A.S. Rao. Your unique manuscript ID is: 9037508.

Please note that during the review process, the submitting author is solely responsible for communicating with the journal and providing any requested updates.

If you believe you were incorrectly listed as a co-author, please contact the editorial office by replying to this email.

Kind regards,
ChemistrySelect

WILEY

Dear Miss Jaya Chandra,

We are pleased to inform you that the manuscript "Novel Thermally-Stable Sr4Zn2W2O12: Sm3+ Phosphors: Synthesis, Optical ,Luminescence properties and Applications in WLEDs" has been submitted to ChemistrySelect by A.S. Rao. Your unique manuscript ID is: 9037508.

Please note that during the review process, the submitting author is solely responsible for communicating with the journal and providing any requested updates.

If you believe you were incorrectly listed as a co-author, please contact the editorial office by replying to this email.

Kind regards,
ChemistrySelect